NASA/TM–2009–214176

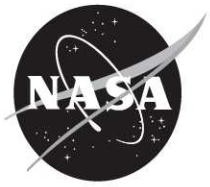

Further Studies on the Physical and Biogeochemical Causes for Large Interannual Changes in the Patagonian Shelf Spring–Summer Phytoplankton Bloom Biomass

Sergio R. Signorini, Virginia M.T. Garcia, Alberto R. Piola, Heitor Evangelista, Charles R. McClain, Carlos A.E. Garcia, and Mauricio M. Mata

February 2009

The NASA STI Program Office … in Profile

Since its founding, NASA has been dedicated to the advancement of aeronautics and space science. The NASA Scientific and Technical Information (STI) Program Office plays a key part in helping NASA maintain this important role.

The NASA STI Program Office is operated by Langley Research Center, the lead center for NASA's scientific and technical information. The NASA STI Program Office provides access to the NASA STI Database, the largest collection of aeronautical and space science STI in the world. The Program Office is also NASA's institutional mechanism for disseminating the results of its research and development activities. These results are published by NASA in the NASA STI Report Series, which includes the following report types:

- TECHNICAL PUBLICATION. Reports of completed research or a major significant phase of research that present the results of NASA programs and include extensive data or theoretical analysis. Includes compilations of significant scientific and technical data and information deemed to be of continuing reference value. NASA's counterpart of peer-reviewed formal professional papers but has less stringent limitations on manuscript length and extent of graphic presentations.
- TECHNICAL MEMORANDUM. Scientific and technical findings that are preliminary or of specialized interest, e.g., quick release reports, working papers, and bibliographies that contain minimal annotation. Does not contain extensive analysis.
- CONTRACTOR REPORT. Scientific and technical findings by NASA-sponsored contractors and grantees.
- CONFERENCE PUBLICATION. Collected papers from scientific and technical conferences, symposia, seminars, or other meetings sponsored or cosponsored by NASA.
- SPECIAL PUBLICATION. Scientific, technical, or historical information from NASA programs, projects, and mission, often concerned with subjects having substantial public interest.
- TECHNICAL TRANSLATION. English-language translations of foreign scientific and technical material pertinent to NASA's mission.

Specialized services that complement the STI Program Office's diverse offerings include creating custom thesauri, building customized databases, organizing and publishing research results . . . even providing videos.

For more information about the NASA STI Program Office, see the following:

- Access the NASA STI Program Home Page at http://www.sti.nasa.gov/STI-homepage.html
- E-mail your question via the Internet to help@sti.nasa.gov
- Fax your question to the NASA Access Help Desk at (301) 621-0134
- Telephone the NASA Access Help Desk at (301) 621-0390
- Write to:
  NASA Access Help Desk
  NASA Center for AeroSpace Information
  7115 Standard Drive
  Hanover, MD 21076–1320

NASA/TM–2009–214176

Further Studies on the Physical and Biogeochemical Causes for Large Interannual Changes in the Patagonian Shelf Spring–Summer Phytoplankton Bloom Biomass

Sergio R. Signorini
Science Applications International Corporation, Beltsville, Maryland

Virginia M.T. Garcia
Federal University of Rio Grande, Rio Grande, Brazil

Alberto R. Piola
Universidad de Buenos Aires, Buenos Aires, Argentina

Heitor Evangelista
Universidade do Estado do Rio de Janeiro, Brazil

Charles R. McClain
NASA Goddard Space Flight Center, Greenbelt, Maryland

Carlos A.E. Garcia and Mauricio M. Mata
Federal University of Rio Grande, Rio Grande, Brazil

National Aeronautics and
Space Administration

Goddard Space Flight Center
Greenbelt, Maryland 20771

February 2009

Available from:

NASA Center for AeroSpace Information
7115 Standard Drive
Hanover, MD 21076-1320

National Technical Information Service
5285 Port Royal Road
Springfield, VA 22161

Abstract − A very strong and persistent phytoplankton bloom was observed by ocean color satellites during September − December 2003 along the northern Patagonian shelf. The 2003 bloom had the highest extent and chlorophyll *a* (Chl-a) concentrations of the entire Sea-Viewing Wide Field-of-view Sensor (SeaWiFS) period (1997 to present). SeaWiFS-derived Chl-a exceeded 20 mg m^{-3} in November at the bloom center. The bloom was most extensive in December when it spanned more than 300 km across the shelf and nearly 900 km north − south (35° S to 43° S). The northward reach and the deep penetration on the shelf of the 2003 bloom were quite anomalous when compared with other years, which showed the bloom more confined to the Patagonian shelf break (PSB). The PSB bloom is a conspicuous austral spring-summer feature detected by ocean color satellites and its timing can be explained using the Sverdrup critical depth theory. Based on high-resolution numerical simulations, *in situ* and remote sensing data, we provide some suggestions for the probable mechanisms responsible for that large interannual change of biomass as seen by ocean color satellites. Potential sources of macro and micro (e.g., Fe) nutrients that sustain the high phytoplankton productivity of the Patagonian shelf waters are identified, and the most likely physical processes that maintain the nutrient balance in the region are discussed. Seasonal and interannual changes in vertical mixing, shelf intrusions of the Malvinas Current, and the position of the Brazil-Malvinas confluence zone, are the most likely mechanisms driving the observed changes in phytoplankton production. Previous studies advocate that the South Atlantic Ocean is the recipient of dissolved Fe from various sources, including, atmospheric deposition from desert dust and volcanic ash, and coastal submarine groundwater discharge from lagoon systems, but the scope of our analysis and data limitations precluded us from establishing a connection between these sources of Fe and the Patagonian shelf bloom. This paper highlights the complexity of the biogeochemical processes that control the shelf biomass and production of the region and provides suggestions for further studies to improve our understanding of the physical-biological interactions responsible for nutrient balance and ecosystem response.

1. Introduction

Along the Patagonian coast off Argentina, the shelf-break front formed between shelf waters and the Malvinas (Falkland) Current (MC) shows a conspicuous band of high phytoplankton biomass throughout spring and summer detected by ocean color sensors. This region is the feeding and spawning ground of several commercial species of fish and squid [*Acha et al.*, 2004] and is thought to play an important role in CO_2 sequestration by the ocean [*Bianchi et al.*, 2005]. The physical and biological characteristics of the Patagonian Shelf Break (PSB) front have been previously investigated [*Acha et al.*, 2004; *Rivas*, 2006; *Rivas et al.*, 2006; *Saraceno et al.*, 2005; *Signorini et al.*, 2006]. The region bordering the PSB presents elevated chlorophyll *a* (Chl-a) from spring through autumn presumably supported by the nutrient-rich subsurface waters of the MC. This nutrient supply is probably a result of upwelling processes caused by the interaction between the MC and the continental slope [*Carreto et al.*, 1995; *Matano and Palma*, 2008]. Near 39°S there is an energetic southward and eastward flow resulting from the collision of the southward Brazil Current (BC) with the MC, namely the Brazil/Malvinas Confluence (BMC). The MC transports cold and relatively fresh sub-Antarctic waters equatorward, and the BMC generates one of the most energetic regions of the world ocean [*Piola and Matano*, 2001]. The BMC extends eastward forming the South Atlantic Current (SAC). The SAC is an eastward conduit of biogenic material originating on the outer shelf and slope through meanders and eddies, as can be seen from satellite images (Figure 1).

It has been suggested that low productivity in nutrient-rich surface waters of the Southern Ocean may result from a deficiency of Fe [*Martin et al.*, 1990]. The MC is a branch of the Antarctic Circumpolar Current (ACC) and thus inherently low in iron concentration. There is *in situ* evidence that the Malvinas upwelling region is a large source of macro nutrients, especially nitrate [*Carreto et al.*, 1995; *Garcia et al.*, 2007], but the origin of Fe to maintain the intense PSB bloom remains elusive due to the sparse *in situ* Fe measurements. *Bowie et al.* [2002] made a few measurements of Fe in the region and reported a maximum of 1.7 nM in the front of the sub-tropical convergence zone towards Uruguay at 35°S. Further south, they found that the total dissolved Fe tended towards baseline values (~0.3 to 1.0 nM), with an increase (2.7 nM) observed in the shelf waters off the East Malvinas Island, but there are very few samples south of 35°S. Two sources of Fe for the surface waters of the Atlantic Southern Ocean (SO) have been proposed [*Cassar et al.*, 2007; *Erickson et al.*, 2003; *Gaiero et al.*, 2003; *Meskhidze et al.*, 2007]: (1) oceanic input from upwelling and lateral flows from continental margins; and (2) atmospheric input from deposition of mineral dust emanating from the arid regions of South America and ash clouds from volcanic eruptions. Regardless of its origin, changes in Fe concentration can significantly alter ocean productivity. With increasing dissolved Fe concentrations, the growth rates of open-ocean SO diatoms can increase several fold [*Timmermans et al.*, 2004].

In this paper we provide evidence of large interannual variability of ocean productivity along the Patagonian shelf, with a very large and anomalously intense bloom occurring in spring-summer 2003. Based on high-resolution numerical simulations and remote sensing data, we provide some suggestions for the probable mechanisms responsible for that large interannual change of biomass as seen by ocean color satellites. Moreover, we focus on the 2003 anomalous event, as it clearly stands out from the region's pattern observed along more the 10 years of satellite ocean color data. However, the physical processes that maintain the overall balance of nutrients and resulting

biogeochemical interactions are not fully understood and further field and numerical studies are needed to better describe the observed phytoplankton variability.

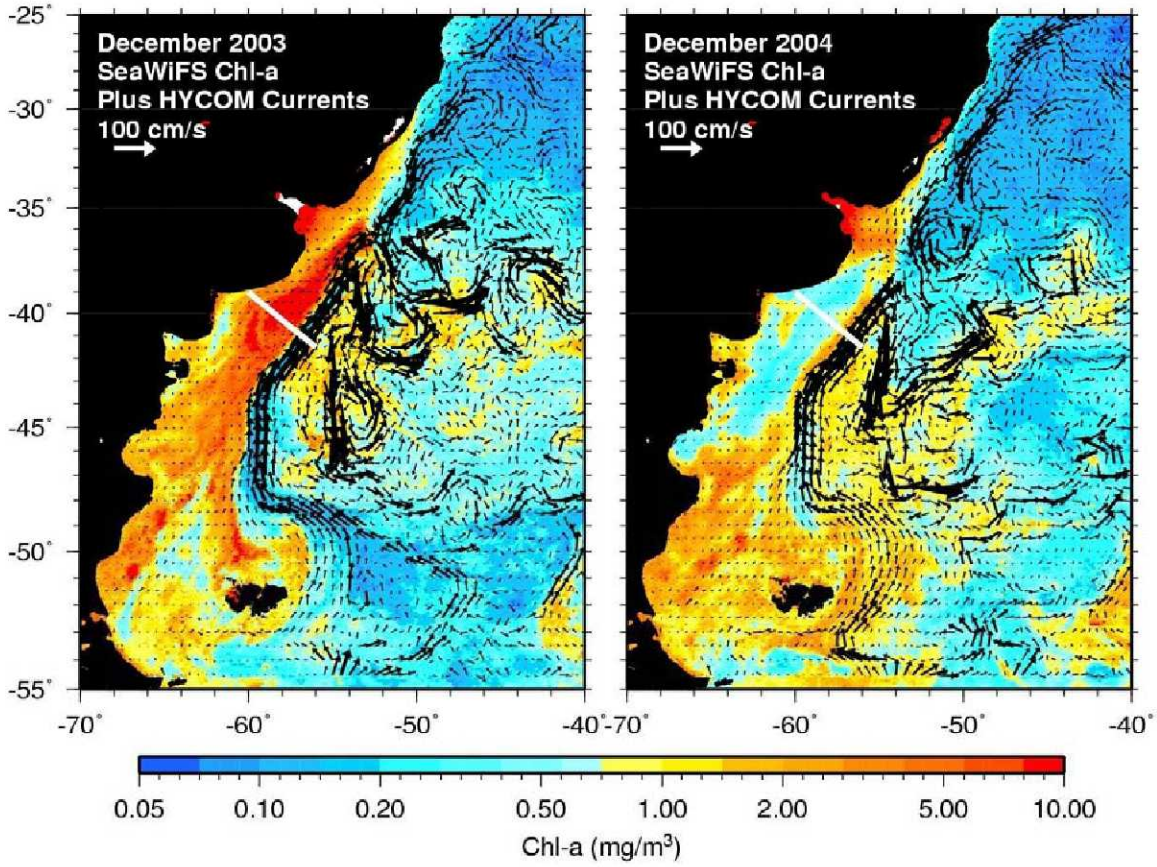

Figure 1. Monthly composites of SeaWiFS Chl-a for December 2003 and 2004. The corresponding HYCOM 30-meter currents are superimposed. The white line indicates the location of the cross-shelf transect used in the analysis.

2. Data Sources and Methodology

2.1 Satellite Data

SeaWiFS Chl-a (production algorithm) and Photosynthetic Available Radiation (PAR) 9-km monthly data, and 4km Moderate Resolution Imaging Spectroradiometer (MODIS) Aqua sea-surface temperature (SST) were obtained from the NASA Ocean Color distribution archive (ftp://oceans.gsfc.nasa.gov/). A calcite, or particulate inorganic carbon (PIC), algorithm [*Balch et al.*, 2005] was used to produce monthly 4-km PIC composites using SeaWiFS Global Area Coverage (GAC) data.

Monthly composites, cross-sections and time series extracts were processed and analyzed. Monthly 4-km Pathfinder Advanced Very High Resolution Radiometer (AVHRR) SST (http://podaac-www.jpl.nasa.gov/) and monthly $0.5^{o}\times0.5^{o}$ Quick Scatterometer (QuikScat) winds (http://www.ifremer.fr/cersat/en/index.htm) were used to derive SST time series and monthly wind and SST anomalies concurrent with the SeaWiFS mission. We used all available concurrent data,

which are limited to September 1997 – December 2006 for the Pathfinder AVHRR SST and August 1999 – September 2007 for QuikScat winds.

2.2 HYbrid Coordinate Ocean Model or HYCOM

HYCOM products (mixed layer thickness, mixed layer velocity components, and sub-surface temperature and salinity) were obtained from the HYCOM data service web site (http://hycom.rsmas.miami.edu/dataserver/). Computations are carried out on a mercator grid between 78°S and 47°N (1/12° equatorial resolution). The horizontal dimensions of the global grid are 4500 x 3298 grid points resulting in ~7 km spacing on average. There are 32 vertical layers. Bathymetry is derived from a quality controlled NRL DBDB2 dataset. Surface forcing is from Navy Operational Global Atmospheric Prediction System (NOGAPS) and includes wind stress, wind speed, heat flux (using bulk formula), and precipitation. We obtained outputs from the hindcast experiment which uses the Navy Coupled Ocean Data Assimilation (NCODA) system for data assimilation (SST, SSH, XBTs, ARGO floats and moored buoys). The hindcast products are available from November 2003 until current. HYCOM is a very mature model and a vast literature is available on its performance, validation, and applications to a variety of ocean basins [*Chassignet et al.*, 2006; *Chassignet et al.*, 2007; *Cheng et al.*, 2007; *Halliwell*, 2004; *Kara and Hurlburt*, 2006; *Kelly et al.*, 2007; *Winther and Johannessen*, 2006].

2.3 Temperature-derived Nitrate

Figure 2a shows the station locations from which the concurrent nitrate and temperature data originated to derive a NO_3 vs. T relationship. Only quasi-synoptic transects that sampled the Brazil and Malvinas Currents and their convergence region were used. A robust regression (r^2=0.93) of nitrate versus temperature (Figure 2b) was developed based on 976 observations from 74 stations available from the NOAA NODC World Ocean Database (http://www.nodc.noaa.gov/OC5/). The regression equation is

$$\log_{10}(NO_3) = -0.003999\ T^2 + 0.009954\ T + 1.488 \qquad (1)$$

Data shallower than 50 m were not used to reduce biases due to biological consumption. Most of the data originated from depths between 50 and 500 m. The goal was to obtain nitrate concentrations resulting from physical transport only. *Carreto et al.* [1995] provided a linear equation (r^2=0.97) of nitrate versus temperature using 32 observations from a cross-shelf transect off Mar del Plata in the Argentinean Sea, but we were not able to apply it to our region since it yields negative retrievals for temperatures greater than 12°C.

3. Results and Discussion

3.1 Evidence of Anomalous Bloom Behavior

A very strong and persistent phytoplankton bloom occurred during September – December 2003 at the northern Patagonian shelf (north of 43°S). The SeaWiFS Chl-a peaked in November and exceeded 20 mg m^{-3} at the bloom center (~ 40.5°S and 58°W). The bloom was widest in December

when it spanned more than 300 km across the shelf and nearly 900 km north − south (35° S to 43° S). In contrast, in December 2004 there was a much weaker bloom confined to the shelf break, which is a more typical behavior for the region. Figure 1 contrasts the December 2003 and 2004 SeaWiFS Chl-a distribution clearly showing the anomalous size and strength of the 2003 bloom.

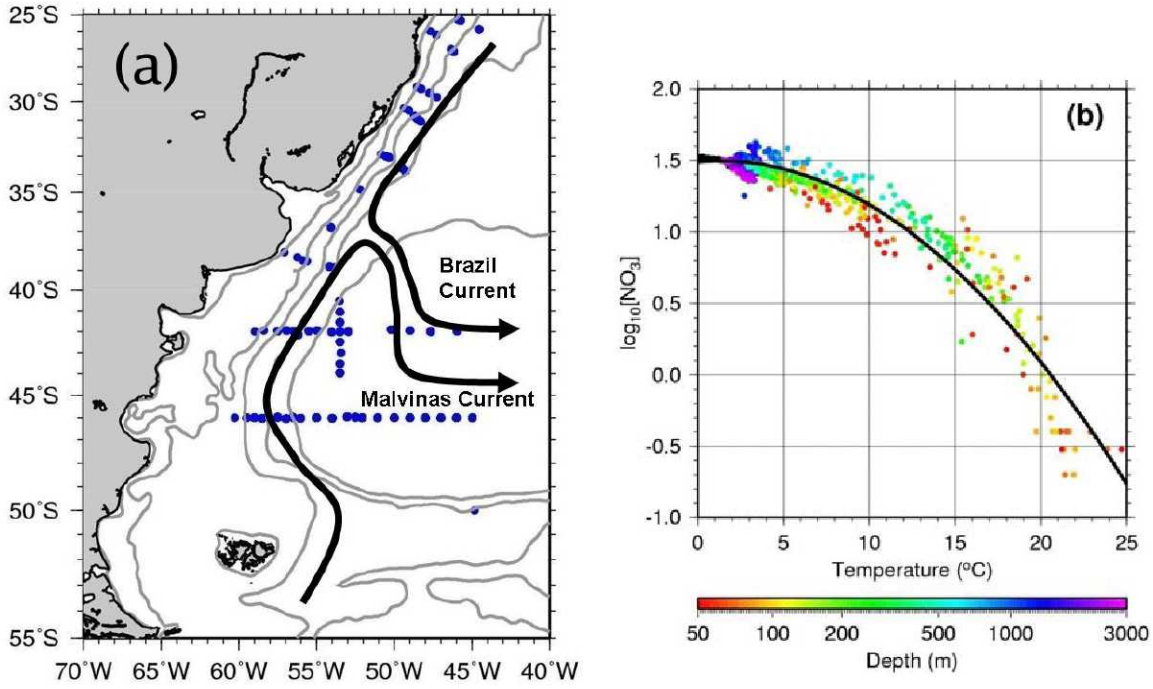

Figure 2. (a) NODC station locations with bathymetry (30, 100, 1000, 3000, and 5000 m) and approximate location of Brazil and Malvinas Currents superimposed. (b) Nitrate polynomial regression ($\log_{10}$ [NO_3] versus temperature) based on 976 *in situ* observations below 50 m depth. The color indicates the observation depth.

Figure 3 shows cross-shelf time series (see Figure 1 for transect location) of SeaWiFS Chl-a and PAR, and surface NO_3 derived from Pathfinder AVHRR SST and equation (1). Cross-shelf average time series are superposed in white and the horizontal black line is the position of the 100 m isobath (shelf break). The bloom seasonal cycle is clearly shown, with peaks during the cross-over of elevated PAR and relatively high NO_3 occurring in November-December. Highest NO_3 levels (> 20 μM) occur in the peak of winter (July-August) in the PSB when Malvinas waters are vertically mixed due to convective overturning and biological consumption is at a minimum. The winter-summer contrast in stratification will be shown later on when HYCOM cross-shelf transects are discussed.

Large interannual variability of Chl-a can be seen in Figure 3. The transect crosses the widest part of the December 2003 bloom and reveals that the bloom was anomalous in its strength, size, and position on the shelf. The normal seasonal cycle of the bloom occurs during the same period but with much lower Chl-a and with peak values more confined to the PSB. Figure 3 also shows that the spring-summer bloom transitioned to more productive conditions in 2002 and returned to more typical conditions in 2005. Note that the strongest bloom confined to the PSB occurred during the spring-summer of November 2002 − January 2003.

The PSB is also characterized by a transition of phytoplankton groups during the spring-summer bloom [*Garcia et al.*, 2007; *Signorini et al.*, 2006]. Although very few samples have been

collected contemporaneously with satellite data to validate ocean color algorithms for this region, a time series image analysis of calcite and chlorophyll algorithms in the shelf-break region indicate that the blooms initiate in austral spring, probably dominated by diatoms, but in mid summer (December, January) the community is mainly represented by calcite-producing (coccolithophores) phytoplankton [*Signorini et al.*, 2006]. Signorini et al. [2006] hypothesize that the transition from diatoms to coccolithophores occurs in mid summer when the mixed layer gets much shallower reducing the nutrient level at surface layers but allowing an increase of light harvesting by phytoplankton. The coccolithophores thrive in high light and low nutrient conditions, while the

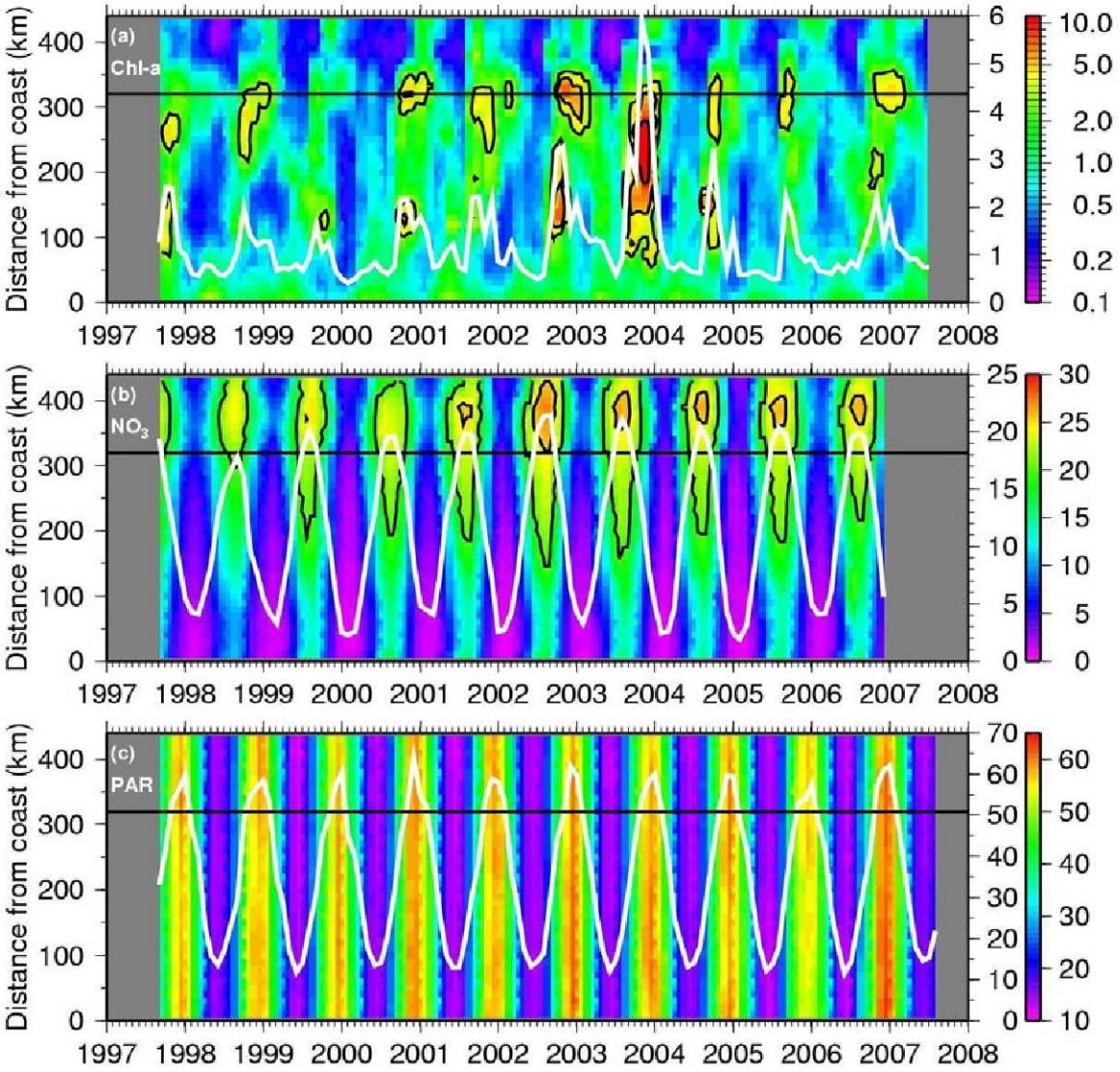

Figure 3. Cross-shelf time series of (a) SeaWiFS Chl-a (mg/m^3), (b) SST-derived surface NO_3 (μM), and (c) SeaWiFS PAR (mol/m^2/d). The black contours are 3, 5, 10 mg m^{-3} for Chl-a and 20 and 25 μM for NO_3. The horizontal black line is the location of the 100 m isobath representing the shelf break. Time series of cross-shelf averages are superposed in white with proper scales on the right of each tier.

diatoms growth is limited under these conditions and a shift from diatoms to coccolithophores gradually occurs. Therefore, the mixed layer thickness plays a major role in this process.

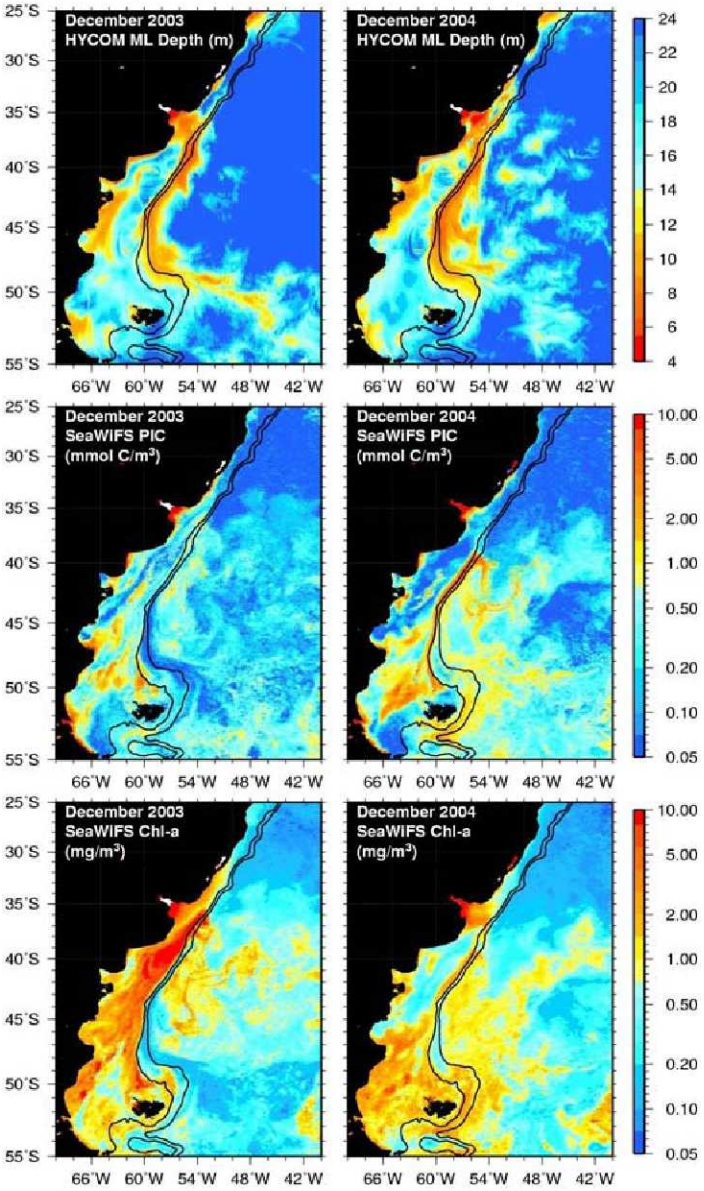

Figure 4. Monthly composites of HYCOM mixed layer thickness, SeaWiFS PIC, and SeaWiFS Chl-a for December 2003 (left column) and December 2004 (right column). The shelf break is represented by the 300 m and 1000 m isobaths.

To better illustrate this hypothesis, Figure 4 shows December 2003 and 2004 composites of HYCOM mixed layer depth (MLD), SeaWiFS-derived PIC concentration, and SeaWiFS Chl-a. The PIC concentration and the coccolithophore flag [*Brown and Podesta*, 1997; *Brown and Yoder*, 1994] used in the Chl-a algorithm are well correlated in space and time [*Signorini et al.*, 2006] suggesting that PIC concentration is a proxy for coccolithophore abundance. Note that there is a band of low MLD following the PSB. This is a result of the summer warming above the shallow thermocline along the MC upwelling zone. Although the accuracy of the HYCOM MLD is unknown for this region, it will be shown later (see Figure 9) that the MLD along the cross-shelf transect during December 2004 was on average 7 m thinner than the MLD during December 2003. This is a large difference since the largest MLD along the cross-shelf transect was about 20 m. This shallower MLD apparently had a positive impact on the coccolithophore production in mid-summer 2004 judging from the relatively high values of PIC (>6 mmol C m^{-3}) along the PSB during December 2004 (Figure 4). Conversely, the PIC concentrations along the PSB were much lower during December 2003, while the Chl-a over the shelf region between 35°S and 45°S were much higher (> 10 mg m^{-3}) than in December 2004. Thus the MLD variability had an impact on the shelf production as well.

3.2 SST, Chl-a, and Wind Anomalies

To further illustrate the anomalous nature of the 2003 bloom, Figure 5 and 6 show the distributions of Chl-a, SST, and wind anomalies for October, November, and December 2003 − 2004, respectively. In contrast with the scalar parameters, caution must be taken when interpreting the wind anomalies (speed and velocity vectors). They are somewhat difficult to interpret as the mean of the speed can be quite different than the mean of the vectors. For instance, variable wind direction at

a particular location may have a high mean speed but almost zero mean vector velocity if the wind direction has a symmetric distribution. Conversely, persistent and steady winds have both elevated speed and vector means. Because of this, the monthly mean wind speed and vectors are also provided in Figure 5 and 6 as a reference. Comparison between Figures 5 and 6 shows interesting contrast in anomaly patterns between spring-summer of 2003 and 2004. During 2003, the shelf region to the south of the Rio de la Plata mouth exhibits large positive anomalies of Chl-a (up to 10 or more mg m^{-3}), negative SST anomalies, and stronger offshore and northerly winds. During 2004 the anomalies of Chl-a and SST reverse showing lower Chl-a and warmer SSTs on the shelf region, especially during December. The winds were parallel to the coast (northeasterly) blowing along the PSB and against the direction of the MC leading to an offshore Ekman transport component. Thus, coastal upwelling is not a primary factor with respect to the 2003-2004 differences. In contrast, the offshore winds during 2003 favored the MC northeastward flow via the Ekman transport, which is most probably the cause for a nearly 2^{o} northward displacement of the BMC as shown in Figure 2. This displacement had an impact on the Chl-a which shows a positive anomaly extending northward up to the latitude of the Rio de La Plata mouth near 35^{o}S. The 2003 cold SST anomalies are in agreement with larger MLDs, especially during December 2003.

3.3 Role of Light on the Timing of the Spring Bloom and the Sverdrup Critical Depth

Sverdrup's critical depth hypothesis [*Sverdrup*, 1953] has been applied to many oceanic and even estuarine ecosystems with the goal of evaluating the roles of light availability and vertical mixing leading to phytoplankton spring blooms [*Nelson and Smith*, 1991; *Obata et al.*, 1996; *Siegel et al.*, 2002; *Townsend et al.*, 1992]. Before the iron hypothesis was introduced, the prevailing idea of the control of primary production in the Southern Ocean was that relatively weak vertical stability and strong winds combined to mix the upper ocean and its resident phytoplankton assemblages over depths that resulted in low time-integrated irradiance for the photosynthetic cells. Following this reasoning, the productivity of most of the Southern Ocean is low even in summer because the depth of the surface mixed layer (*Zm*) approaches or exceeds the Sverdrup critical depth (*Zcr*). This depth is a function of the solar irradiance at the sea surface, the clarity of the water, and the phytoplankton compensation irradiance (irradiance at which photosynthesis equals respiration rates). This simplified formulation assumes that the mixed layer is not nutrient-limited and that there are no grazing or other losses. The *Zcr* equation is as follows

$$\frac{Zcr}{\left(1-\exp(-K\,Zcr)\right)} = \frac{I_o}{K\,I_c} \qquad (2)$$

where I_o is the incident PAR at the surface, K is the diffuse attenuation coefficient for PAR, and I_c is the average irradiance for the water column that equals the compensation irradiance. Sverdrup defined the critical depth as the depth at which the vertically integrated rates of plankton photosynthesis and respiration are equal. Therefore, when $Zm > Zcr$, the vertically integrated rate of phytoplankton photosynthesis is less than that needed to keep pace with consumption of organic carbon from respiration. Under these conditions net phytoplankton biomass cannot take place. Conversely, when $Zm << Zcr$, production exceeds respiration and the phytoplankton assemblages flourish. With the above criteria and assumptions in mind, we applied the critical depth analysis to the Patagonian shelf bloom. The value of *Zcr* calculated from equation (2) is subject to large uncertainties for several reasons.

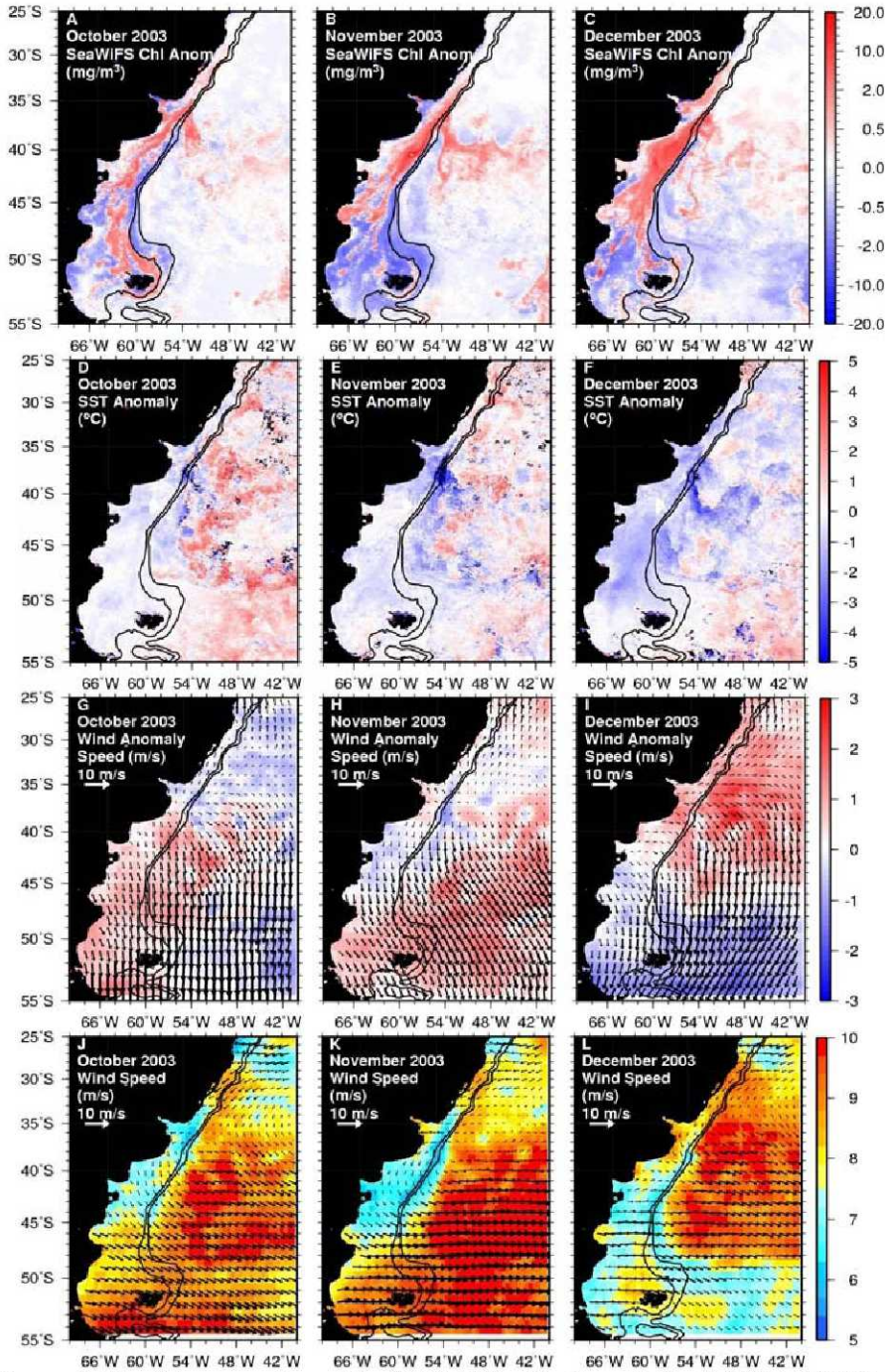

Figure 5. Monthly anomalies of SeaWiFS Chl-a (A, B, and C), AVHRR SST (D, E, and F), and QuikScat wind speed and vectors (G, H, and I) for October, November and December 2003. QuikScat absolute monthly wind and vectors are shown at the bottom (J, K, and L).

In the original Sverdrup formulation I_o is taken as total solar irradiance rather than PAR. There are several other losses involved other than respiration, such as sinking, grazing, and release of dissolved organic material (DOM). Although not all uncertainties can be reduced or eliminated, Nelson and Smith [1991] reformulated equation (2) by substituting terms that are more consistent with 'present-day' optical and biological data while still preserving the Sverdrup's original logic and mathematics. Using their reformulated equation, they investigated the control of Southern Ocean (including the ACC) productivity by the irradiance-mixing regime. The reformulated equation for *Zcr* is

$$Zcr = \frac{I_o}{3.78\,K} \qquad (3)$$

where the coefficient 3.78 is a result of a series of transformations, including a 20% surface PAR reduction due to surface reflectivity, but is the equivalent of I_c in units of mole quanta m^{-2} day^{-1}, which are the same units of I_o. K is in m^{-1} and *Zcr* in m. They also used the following empirical relationship first proposed by Riley [1956] for K dependence on chlorophyll for systems where most absorbance of irradiance is by water and chlorophyll

$$K = 0.040 + 0.0088(Chl) + 0.054(Chl)^{2/3} \quad (4)$$

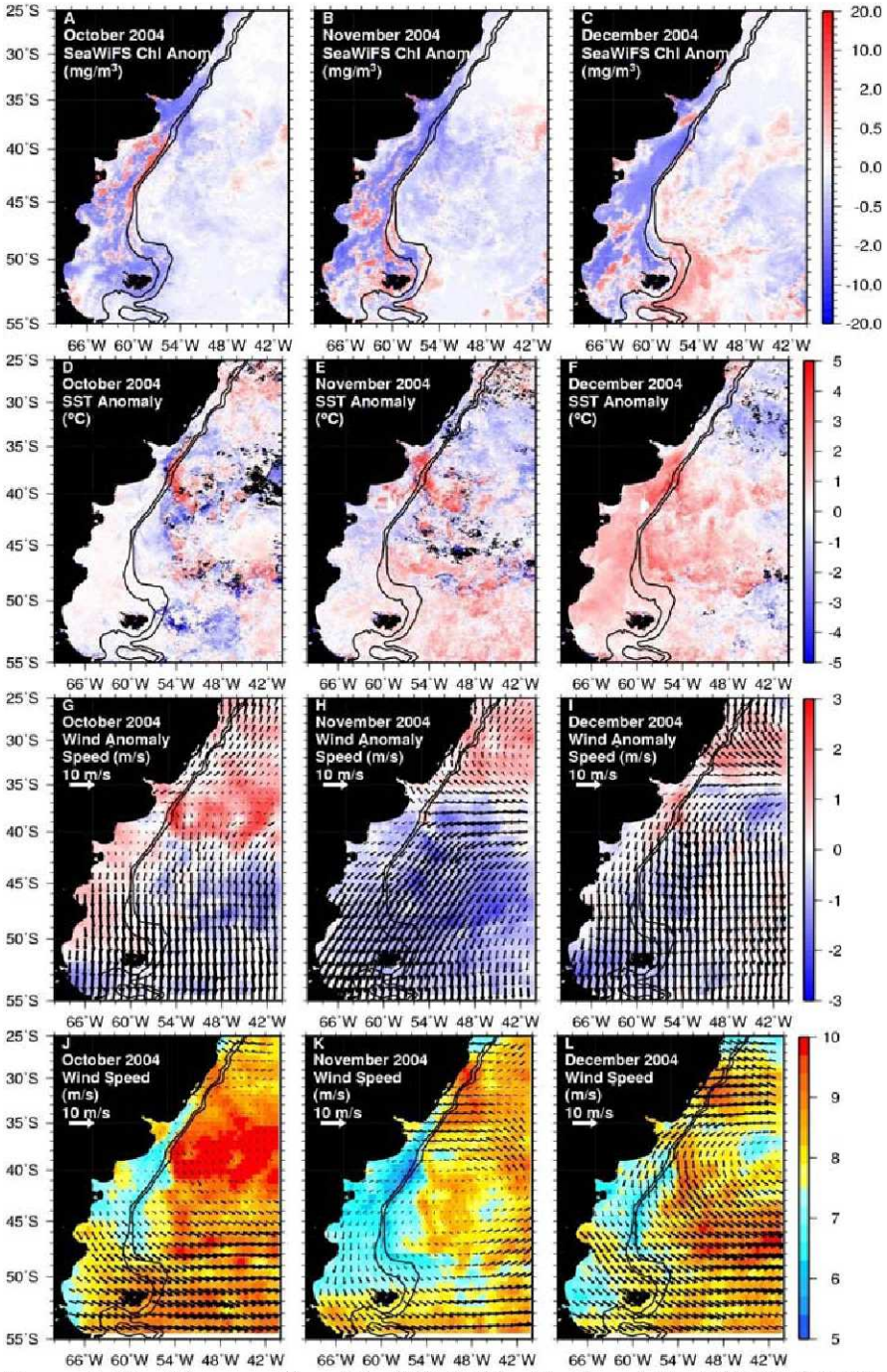

Figure 6. Monthly anomalies of SeaWiFS Chl-a (A, B, and C), AVHRR SST (D, E, and F), and QuikScat wind speed and vectors (G, H, and I) for October, November and December 2004. QuikScat absolute monthly wind and vectors are shown at the bottom (J, K, and L).

Using equations (3) and (4), monthly MLD climatologic fields from NODC, and SeaWiFS Chl-a and PAR monthly products, we produced a monthly time series climatology of cross-shelf averaged (see Figure 1 for transect location) *Zm* (MLD), Chl-a, and *Zcr*. The average was conducted from the coast to ~340 km offshore to include the shelf and the MC upwelling zone. The seasonal time series is shown in Figure 7. Inspection of this figure reveals a classical behavior of the spring bloom. During winter, *Zm* exceeds or approaches *Zcr*, the time-integrated irradiance for photosynthesis is low, and despite elevated nutrients within the relatively deep MLD, production is low (Chl-a $\approx$ 0.8 mg m^{-3} on average). Around August-September, there is a fast decrease in *Zm* and a simultaneous large increase in *Zcr*, the mixed layer becomes shallower and still nutrient rich and the spring bloom occurs with peak production (Chl-a $\approx$ 2.6 mg m^{-3} on average) around November. The mixed layer stays relatively shallow (< 20 m) until February but the intense spring bloom consumes most of the nutrients by December-January, and a steep shallow thermocline prevents a steady nutrient input from below. Therefore, production quickly decreases and by autumn biomass returns to its background value of less than 1.0 mg m^{-3} of Chl-a. This

scenario clearly shows that the Sverdrup critical depth model explains the mechanisms that drive the timing of the Patagonian shelf spring bloom.

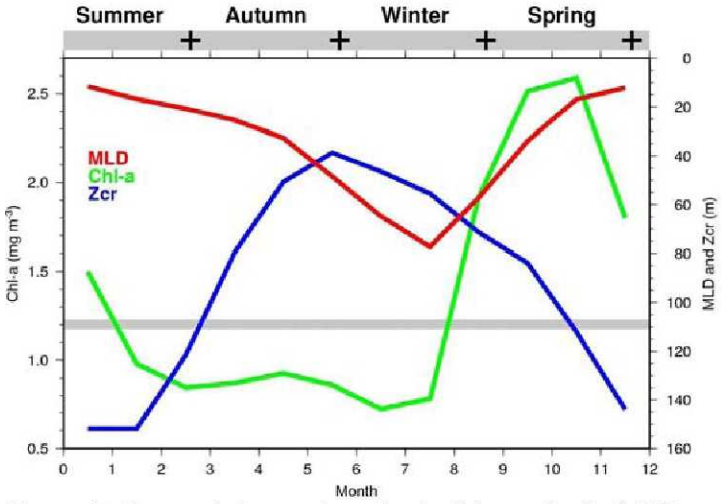

Figure 7. Seasonal time series of mixed layer depth (MLD, or *Zm*), Chl-a, and Sverdrup critical depth (*Zcr*). The thick grey line represents the average depth (~108 m) across the shelf and shelf break.

3.4 Subsurface Cross-Shelf Transects

Subsurface cross-shelf transects of monthly temperature, salinity, and temperature -derived nitrate for January (summer) and July (winter) 2004 are shown in Figure 8. The temperature and salinity fields originate from the HYCOM 2003 – 2004 hindcast run, while the nitrate was obtained from the HYCOM temperature field and equation (1). Transects of monthly SeaWiFS Chl-a and MODIS SST are also shown. The red line on each of the subsurface fields is the monthly MLD, also obtained from the HYCOM run, while the blue line represents the Sverdrup critical depth. Note the large difference in temperature stratification between summer and winter. There is no vertical salinity stratification in winter or summer since there are no large freshwater sources along the Patagonian coast. The shelf is highly temperature-stratified during summer while the thermocline is very shallow at the PSB (~20 m based on the 11°C isotherm depth). Nitrate concentrations over the shelf range from 1 to 4 μM, with cross-shelf gradients indicating that the MC subsurface intrusion is the likely nitrate source. The MLD is less than 20 m across the whole transect. Conversely, during winter, the whole shelf is mixed almost all the way to the bottom, the thermocline over the shelf break is much deeper, and nitrate concentrations over the shelf range from 12 to 20 μM.

These HYCOM-derived cross-shelf parameters (T, S, NO_3) are reasonably similar to the values obtained by Carreto et al. [1995] from *in situ* data along a cross-shelf transect offshore of Mar del Plata (38°S – 40°S) for the same months, except for salinity being fresher nearshore in their data due to the proximity to the Rio de La Plata mouth. In addition, the derived nitrate using HYCOM temperatures does not include by definition the biological uptake during the spring bloom and thus overestimates summer nitrate within the mixed layer. The *Carreto et al.* [1995] transects revealed that a very strong and shallow (20 – 30 m) thermocline and nitracline developed during February and March 1989 with nitrate values much less than 1 μM above it. Chlorophyll subsurface maxima of 2.0 mg m^{-3} occurred at the nitracline depth. The chlorophyll stratification during the previous spring (October-November 1988) was quite different, with surface values across the shelf ranging from 2 to 7 mg m^{-3}, and decreasing to less than 1 mg m^{-3} around 50 m.

Note that the mixed layer depth (*Zm*, red line) exceeds or is equal to the Sverdrup critical depth (*Zcr*, blue line) in July and Chl-a is relatively low across the shelf, while in January the *Zcr* far exceeds *Zm* and Chl-a is much higher (up to 6.0 mg m^{-3}), in accordance with the discussion given in the previous section. Also note that in January 2004 the minimum Chl-a occurs near 380 km offshore near the MC upwelling zone where the MLD is shallowest. This is probably a result of the faster nutrient depletion in surface waters by the spring bloom within the shallow MLD. However, it

has to be considered that satellite estimates correspond to chlorophyll in surface layers and, therefore, sub-surface peaks can occur which are not accounted for in our analyses. Note that, according to Figure 8, the nitrate isolines bend towards the surface near 380 Km offshore and this may have an effect on sub-surface phytoplankton growth.

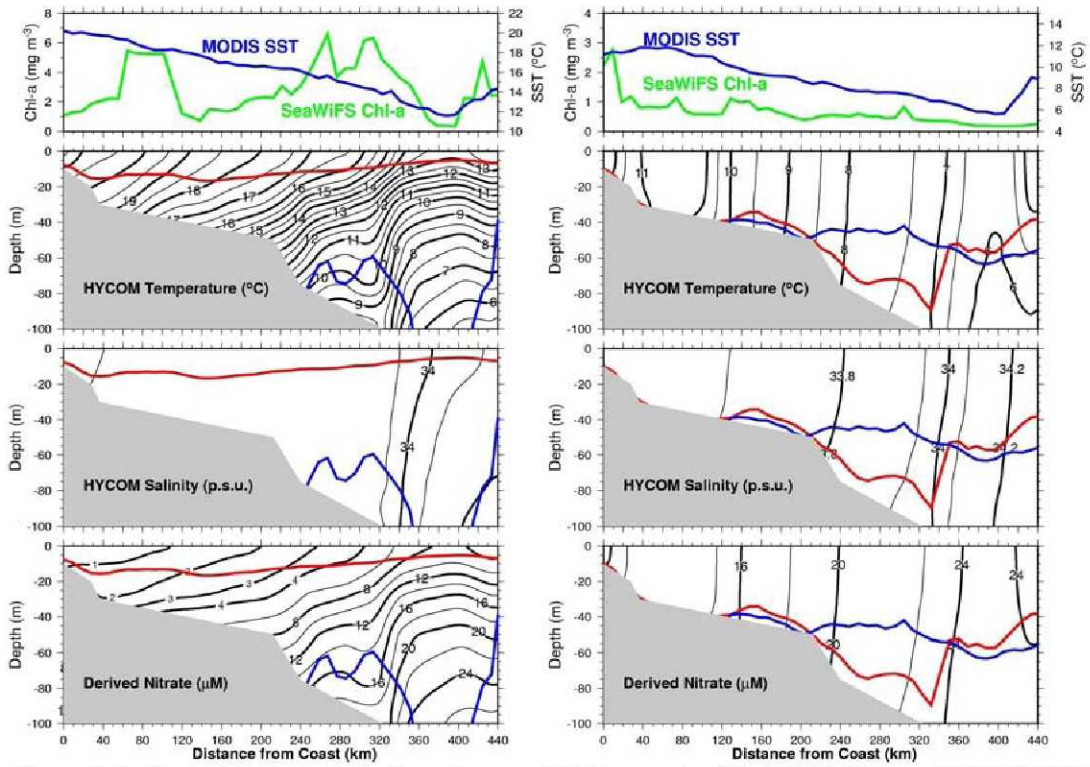

Figure 8. Left panel from top to bottom: January 2004 transects of SeaWiFS Chl-a and MODIS SST, and subsurface HYCOM temperature (*T*), salinity (*S*), and temperature-derived nitrate (NO_3) along the cross-section shown in Figure 1. The red line on the *T*, *S*, and NO_3 cross-sections is the mixed layer thickness, while the blue line is the Sverdrup critical depth (*Zcr*). Right panel: same as left panel, except for July 2004. Note that the Chl-a and SST scales for January 2004 and July 2004 are different.

To better illustrate the differences between the 2003 and 2004 bloom, Figure 9 shows the same fields, except for the addition of PIC, shown in Figure 8 but for December 2003 and 2004 instead. The most striking difference between the two years is that during 2003 the bloom occupied the entire shelf with Chl-a concentrations ranging from 2 to more than 12 mg m^{-3}, while in 2004 the shelf Chl-a concentrations were mostly below 1 mg m^{-3}, except in the MC upwelling zone where Chl-a exceeded 2 mg m^{-3}. The opposite occurred with PIC concentrations that were much less than 2 mmol C m^{-3} in 2003 but greater than 20 mmol C m^{-3} in 2004 at the PSB. One possible, and perhaps most probable, explanation for these differences is the control of productivity by the irradiance-mixing regime. The MLD during December 2003 was on average 7 m deeper than in December 2004. This is a reflection of 2°C colder SSTs, on average, occurring during December 2003. During December 2003 the SST ranged from 9.6°C to 17.3°C with a mean of 13.6°C, while in December 2004 they ranged from 12.0°C to 18.6°C with an average of 15.6°C. Note also that the *Zcr* is much deeper than *Zm*, but more so during December 2004, which is not shown because it exceeds 100 m. As explained before, a critical condition for the onset of the spring bloom is *Zcr* >> *Zm*. However, the shallower the mixed layer the faster the nutrients are consumed and new nutrient supply is

greatly reduced. Simple integration of available total nitrate on the shelf revealed that the difference between 2003 and 2004 was less than 10%, so the higher productivity during December 2003 cannot be accounted for by changes in apparent nutrient supply from the MC at the PSB. Although the dynamics of nutrient uptake and supply cannot be inferred from the available data to ascertain the role of nutrients in the 2003 bloom, vertical mixing and advection seem to be the most probable physical explanation. Note that the PIC concentration, a proxy for coccolithophore presence, is

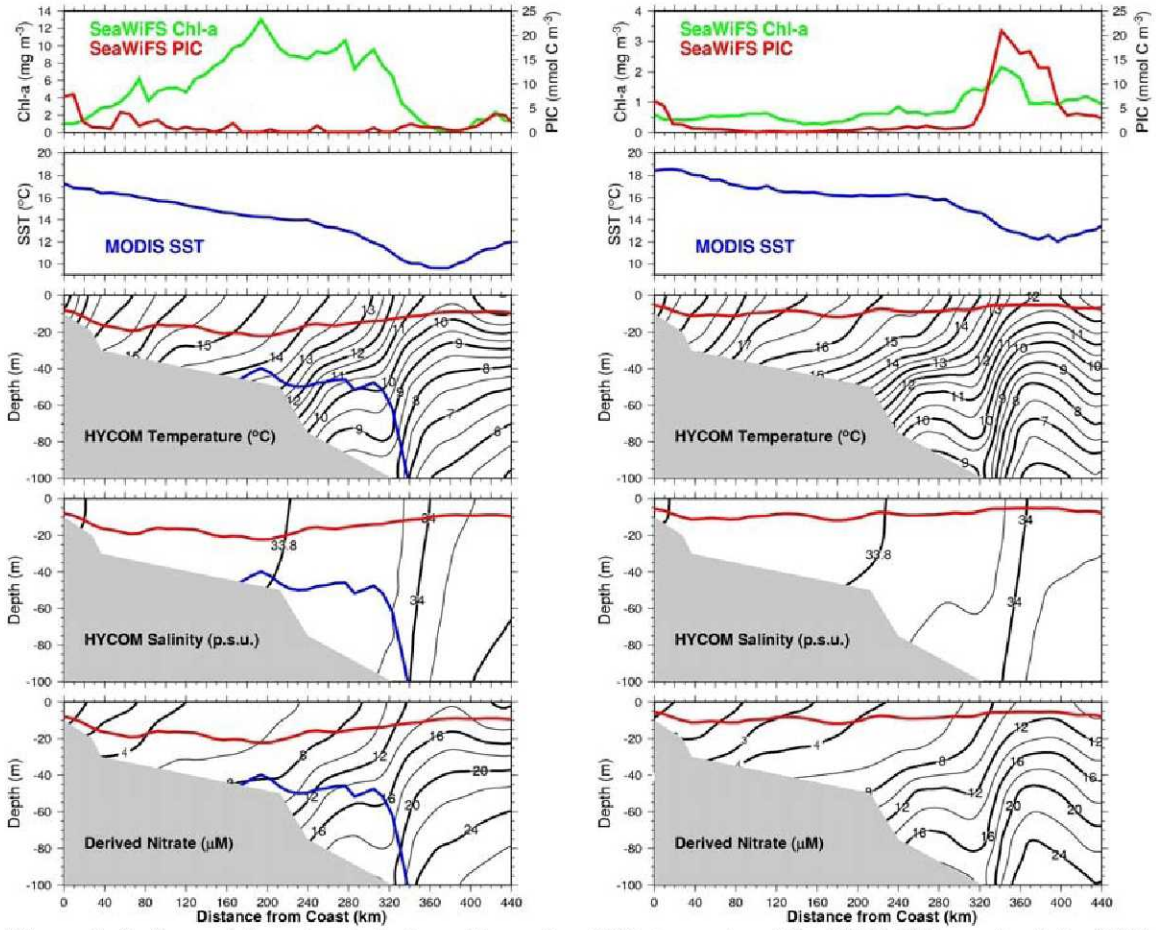

Figure 9. Left panel from top to bottom: December 2003 transects of SeaWiFS Chl-a and calcite (PIC), MODIS SST, and subsurface HYCOM temperature (*T*), salinity (*S*), and temperature-derived nitrate (NO_3) along the cross-section shown in Figure 1. The red line on the *T*, *S*, and NO_3 cross-sections is the mixed layer thickness, while the blue line is the Sverdrup critical depth (*Zcr*). Right panel: same as left panel, except for December 2004. Note that the Chl-a scale for December 2003 and 2004 are different. Also note that the *Zcr* does not show on the December 2004 (right panel) cross sections as it is deeper than 100 m.

highest at the PSB during 2004 where the MLD is shallowest. This is in agreement with our previous reasoning regarding the succession of phytoplankton groups, e.g., diatoms and dinoflagellates followed by coccolithophores.

3.5 Iron Sources and Possible Transport Mechanisms Conducive to Elevated Biomass

The origin of macro-nutrients, especially nitrate, that support the intense blooms in the Patagonian shelf and shelf break can be traced to the MC upwelling and subsurface intrusions onto the shelf. In fact, modeling studies show that MC upwelling can be fairly intense in the Patagonian shelf-break [*Matano and Palma*, 2008]. It is also conceivable, and ecologically required, that sufficient dissolved and bioavailable Fe originates from the MC upwelling zone but the actual Fe concentrations in water remain unknown due to the lack of sufficiently dense *in situ* observations to sample the relatively narrow MC. However, comprehensive field studies [*Niencheski et al.*, 2007; *Windom et al.*, 2006] along the Patos-Mirim lagoon system revealed a large, previously unrecognized source of dissolved iron to the South Atlantic Ocean via submarine ground water discharge (30.5°S to 32.5°S). These studies revealed that the iron flux from these lagoons to the coastal ocean is equal to about 10% of the soluble atmospheric Fe flux to the entire South Atlantic Ocean, implying that its effect on the Patagonian shelf could be potentially large. However, how this source correlates to the 2003 anomalous bloom situation is difficult to determine.

Shelf sediment resuspension may also contribute to dissolved Fe inputs to the water column as shelf sediments tend to accumulate organic and inorganic compounds that sink down from the euphotic zone. Also, the MC may entrain dissolved Fe near the shelf break east of the Malvinas Islands (Falklands), a region that has been previously identified as having relatively high dissolved Fe [*Bowie et al.*, 2002]. Note in Figures 1 and 4 that the bloom around the Malvinas Islands in 2004 was much more intense in size and magnitude than in 2003. If the MC is an important Fe source, the bloom around the Malvinas in 2004 may have depleted the local dissolved Fe concentrations, thus significantly reducing its transport northward by the MC.

Interannual changes in mixed layer depth, especially during spring-summer, MC upwelling and location of the BMC can all contribute to changes in the Patagonian shelf production and biomass. Another possible Fe source is the coastal region off the southern end of South America where the astronomical tides are very strong (promoting intense shelf mixing), and the rivers and glaciers discharge terrigenous dissolved materials onto the shelf. The strong MC advection may capture and transport these materials northward.

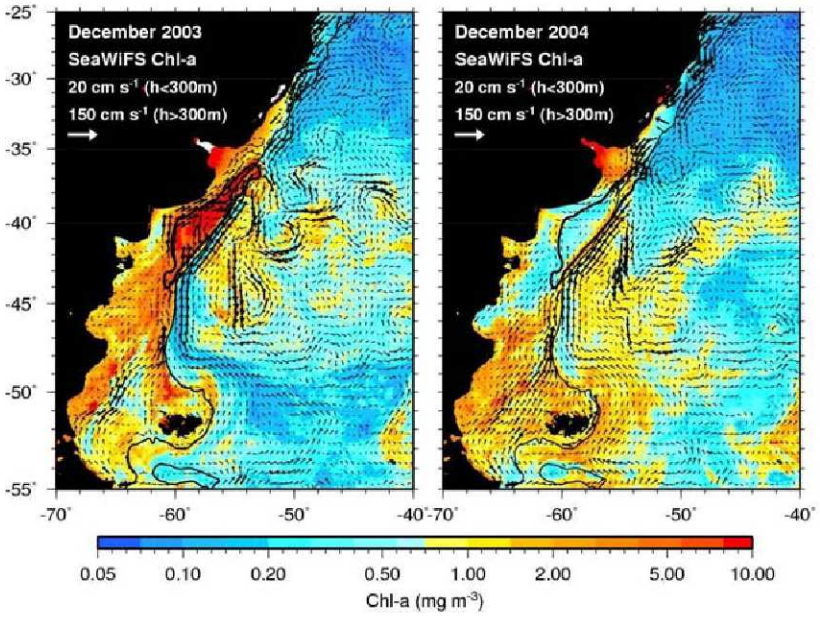

Figure 10a. SeaWiFS monthly composites of Chl-a for December 2003 (left) and December 2004 (right). Equivalent HYCOM currents averaged over 0 − 40 m are superimposed. Note that the vector scales are different for depths (h) less and greater than 300 m. The black contour on the shelf between 36°S and 44°S is the 5 mg m^{-3} Chl-a contour for December 2003, which is repeated for December 2004 as a reference. The 300 m bathymetry contour is also shown.

Figure 10 compares the circulation and water masses present on the PSB and inner shelf between December 2003 and 2004. Figure 10a shows the monthly SeaWiFS Chl-a and upper 40 meters HYCOM mean currents for the two Decembers. During December 2004, a deflection of the MC is clearly shown in the inner shelf from 37°S to 43°S. A MC branch carrying slope waters deflected inshore from the PSB and a region of Chl-a above 5 mg m^{-3} (black contour) resided on the shelf between the shoreward limit of the deflection and the PSB. Figure 10a clearly shows that there was no MC deflection during December 2004 and the Chl-a concentrations within the same region of the shelf were below 0.5 mg m^{-3}. Although there is indirect evidence that these MC deflections may be topographically induced [*Franco et al.*, 2007, in press], it is possible that the 2003 deflection was one of the strongest during the SeaWiFS period. However, since the HYCOM simulation is only available for the period of November 2003 – December 2004, it is not possible to ascertain the anomalous nature of the December 2003 MC deflection.

Further evidence of the effect of the MC deflection on the shelf bloom is provided in Figure 10b, which shows a T-S diagram using values obtained from HYCOM monthly averaged temperature and salinity at all available depths within the bounds of the Chl-a 5 mg m^{-3} contour. The T-S points are shown for December 2003 (circles) and December 2004 (crosses). The labels SASW and STSW indicate the approximate T-S characteristics of the Subantarctic Shelf water and Subtropical Shelf Water, respectively, as described by Piola et al. [2000]. During December 2003, the shelf region where the bloom developed was highly influenced by the colder and fresher SASW, while during December 2004 the same shelf region was predominantly influenced by the warmer and saltier STSW. The colder SASW appears to originate from the outer shelf and the western edge of the MC (Figure 10a) and thus carrying higher nutrient concentration. Thus, it is quite possible that an inshore deflection was a major supplier of nutrients for the anomalous 2003 bloom. The northward displacement of the BMC, combined with SASW shelf intrusion caused by the deflection, have therefore a significant impact on the interannual variability of biomass on the Patagonian shelf.

Another mechanism capable of elevating the Patagonian shelf biomass is the atmospheric deposition of Fe, which can originate from desert dust or volcanic ash. This fertilization from above is much harder to demonstrate since it requires sophisticated measurements of particle fallout at the ocean's surface during hard to predict dust or volcanic ash events. Another difficult aspect is to determine the quantity of soluble Fe present during a given fallout event. Even so, previous studies provided evidence that dust and volcanic ash may play a significant role in the Fe fertilization of the southern ocean, albeit uncertainties regarding this process still abound.

At southern South America, there is only scarce aerosol elemental composition data based on continuous atmospheric monitoring. Once these data are more abundant, they can be used to identify associations between the semi-arid Patagonian desert dust emission and the Patagonian shelf-break primary production. Presently, only models and remote sensing data have provided evidence of a possible association between the two above parameters [*Erickson et al.*, 2003; *Gasso and Stein*, 2007]. Dust measurements conducted in Patagonia, reported by Gaiero et al. [2003], have clearly shown a significant correlation between the total aeolian dust flux and the iron suspended in the local atmosphere (R^2=0.95). Nevertheless, the total flux of dust onto the South Atlantic Ocean remains uncertain. Modeled data have estimated a range from ~0.20 mmol Fe/m^2/yr [*Duce and Tindale*, 1991] to ~10 mmol Fe/m^2/yr [*Tegen and Fung*, 1994]. Considerations on the dissolved fraction of iron (DFe), which is effectively bioavailable to the marine biota, are also based on scarce data: Duce and Tindale [1991] estimated that for the South Atlantic, DFe flux into the ocean would be ~0.08 10^{12}g/yr, considering a conservative model where 10% of the iron dissolves in the sea. In addition, it is believed that chemical transformation and solubilization of the iron may occur during the aerosol

form, along the transport of dust from the desert site to the ocean, due to photochemical reactions and/or the effect of the acidic atmospheric environment. In the remote Southern South American continent, over Patagonia, acidic effect is unlikely to occur regarding the long distances with respect to main South American industrialized regions.

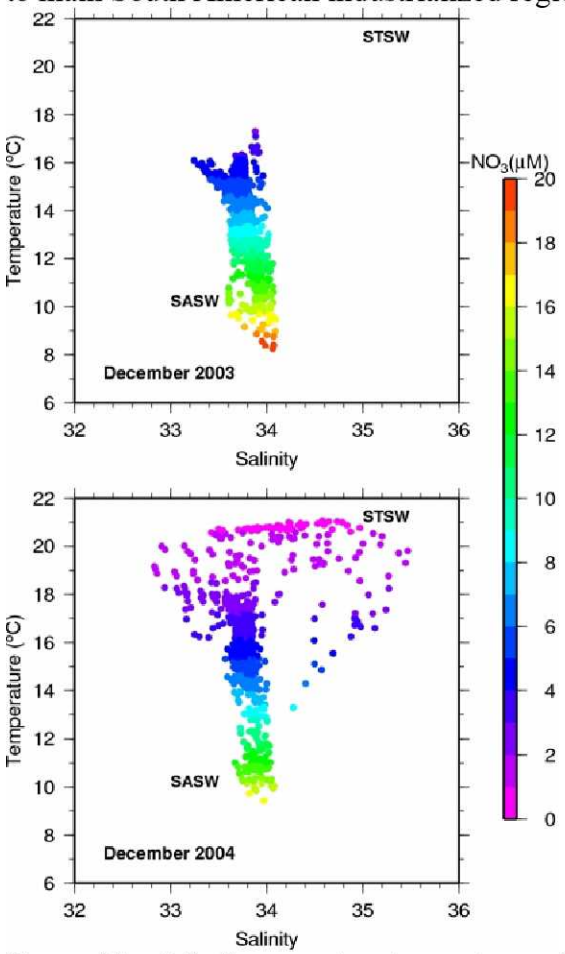

Figure 10b. T-S diagram using temperature and salinity values from HYCOM within 0 – 50 m and inside the region bound by the 5 mg m^{-3} shown in Figure 10a. Note that the nitrate (NO_3) concentration derived from Equation (1) is represented by the color scale. The labels SASW and STSW indicate the approximate T-S characteristics of the Subantarctic Shelf water and Subtropical Shelf Water, respectively, as described by *Piola et al*. [2000].

Nevertheless, the oxidized sulfur (SO_x=SO_2 + sulfate) has been deemed recently as one of the most important chemical atmospheric species in the Southern South America region due to its acidification properties and potential Fe solubility effects. The source stems from combined effects of the numerous active volcanoes along the Chilean Andes, the copper concentrate smelters, and the emissions of at least two megacities: Santiago with ~ 7 million habitants and Buenos Aires with ~12 million habitants. Unlike North America and Europe that started reduction of SO_2 emissions from fossil fuel combustibles since the 1970s, petroleum byproducts employed in South America are still enriched with sulfur. Just before the October – December 2003 bloom, during the austral winter months of August-September 2003, a small eruption with Volcanic Explosivity Index or VEI = 0-1, took place at the Nevados de Chillán Volcanic Complex (36°50'S) [*Naranjo and Lara*, 2004]. This event was potentially able to compose a combined contribution of desert dust and volcanic ash clouds. Although the VEI value does not represent an intense volcanic event (VEI scale varies from 0 to 8 and correspond to plume height restricted to the boundary layer), two aspects may be taken into account: (1) the eastern predominance of winds (from Andes to the Atlantic Ocean) at the low levels, which is favorable to dust delivery into the South Atlantic; and (2) the relative proximity of the Andean Volcanic arc with the Patagonian Shelf-break. Although the event of 29 August 2003 was of relatively low magnitude, volcanic plumes can travel short continental distances before reaching shore areas in the Atlantic Ocean. Figure 11 shows daily dispersion of one-hour, near-tropospheric integration of total ash and plume trajectory inferred from NOAA's HYSPLIT Model between 30 August 30 and 2 September 2003. The impact over the South Atlantic is evident, even though there is a lack of precise data on emission factors.

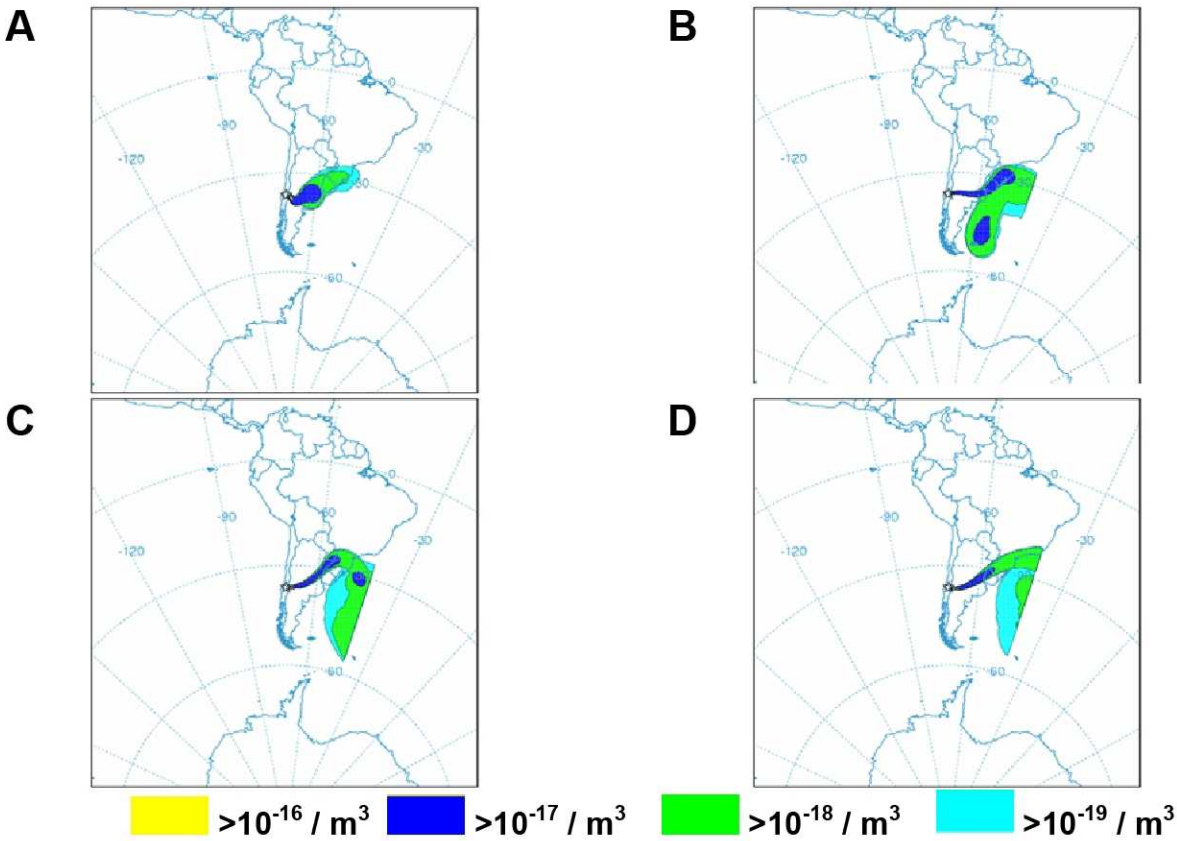

Figure 11. Plume dynamics inferred from NOAA HYSPLIT Model from 2003 eruption at Nevados de Chillán. Plume positions in A, B, C and D correspond to days: August 30th, August 31st, September 1st and September 2nd, respectively. Concentration scale represents a relative value based on total emission.

Iron in volcanic ash (differently from the desert dust) is composed of both iron oxides Fe_2O_3 and FeO, the second form constitute the soluble Fe(II) and in many geochemical analysis of Chilean volcanic ashes, its relative abundance may reach 2-3 times higher than the first form, which is the insoluble form Fe(III). Also, volcanoes are sources of SO_2, which can promote pH acidification of clouds and lead to desert iron solubilization, independently of a soluble iron volcanic source. Therefore, despite the lack of in situ verification, Fe enhancement via atmospheric deposition during the 2003 anomalous bloom cannot be ruled out. The anomalous nature of the bloom may have been a result of a combination of physical factors, including the deflection of the MC onto the shelf and Fe atmospheric deposition.

3.6 Further Investigation of Physical-Biogeochemical Interactions using Analytical and Numerical Models

Additional analyses consisted of:

1) Use of higher time resolution datasets, 8-day for satellite data and daily for HYCOM. Also, products from the biogeochemistry/ecosystem/circulation (BEC) model of *Moore et al.* (2004) were used.

2) Evaluation of nutrient transport onto the shelf based on daily time series of HYCOM *u, v* velocity components and derived nutrients from daily HYCOM temperature (*T*) and salinity (*S*, for silicate only).

3) Time series of phytoplankton growth were obtained using two methods, satellite-derived and model-derived.

3.6.1 Nitrate Onshore Flux

Figures 12 and 13 show MODIS *Chl-a*, HYCOM currents, and HYCOM-derived nutrient distributions for November 2003 and September 2005, which correspond to the highest and lowest biomass along the cross-shelf transect during the peak of the annual phytoplankton bloom, respectively. Figure 14 shows the nutrient regression equations. Only the nitrate onshore flux was computed.

In finite difference form, the components of the nutrient flux (F_x, F_y) at a given model grid point are given by

$$F_x = u(i,j)\frac{\mathrm{NO_3}(i+1,j)-\mathrm{NO_3}(i-1,j)}{2\Delta x}$$
$$F_y = v(i,j)\frac{\mathrm{NO_3}(i,j+1)-\mathrm{NO_3}(i,j-1)}{2\Delta x} \qquad (5)$$

where *u* and *v* are the velocity components, NO_3 the nitrate concentration, dx and dy are the grid cell widths in the east and north directions. The onshore nitrate flux was computed by rotating the flux components 45°, the local orientation of the 100 meter isobath, to obtain the cross-isobath flux.

Figure 15 shows a map of the study region indicating the along-shelf transect near the 100 meter isobath where the onshore nitrate flux was calculated. The estimated annual mean onshore nitrate flux is 1.5×10^5 mol m^{-2} yr^{-1}. Figure 16 shows time series of SeaWiFS *Chl-a* averaged along the cross-shelf transect, onshore nitrate flux, and mean mixed layer nitrate along the same transect (blue line in Figure 15). Inspection of Figure 16 does not reveal any significant increase in onshore nitrate flux during the peak of the 2003 anomalous bloom.

3.6.2 Phytoplankton Carbon Biomass and Growth using the Carbon-based Production Model

The following analysis is based on the Carbon-based Productivity Model (CbPM) described in *Behrenfeld et al.* [2005] and *Westberry et al.* [2008].

The satellite-derived phytoplankton carbon biomass (C_{SAT}) is given by

$$\mathrm{C_{SAT}}(\mathrm{mgC\ m^{-3}}) = SF\left[b_{bp}(443) - b_{bp}(443)_{\mathrm{NAP}}\right] \qquad (6)$$

The scaling factor (*SF* = 13000 mg-C m^{-2}) was derived such that the resulting C is ~25-40% of total POC as estimated using the same backscatter values. The value for $b_{bp}(443)_{NAP}$, 0.00035 m^{-1}, which is the correction for contributions due to a background of nonalgal backscattering particles,

was estimated by type II regression of monthly mean satellite-derived values of $b_{bp}(443)$ and *Chl-a* (see *Behrenfeld et al*., [2005]).

The satellite-derived phytoplankton growth (μ_{sat}) is given by

$$\mu_{\mathrm{SAT}}(\mathrm{d}^{-1}) = \mu_{\max} \frac{Chl/\mathrm{C}_{\mathrm{SAT}}}{(Chl/\mathrm{C})_{\mathrm{N\text{-}Tmax}}} \left[1 - e^{-5Ig}\right] \tag{7}$$

The constant $\mu_{\max}$, assumed to be 2 d^{-1}, approximates the observed maximum growth rate for a natural phytoplankton population (*Banse*, 1991). The physiological response to light (photoacclimation) is characterized by a decreasing exponential function of light. More specifically, it results from a least squares fit of the satellite-derived *Chl*:C distribution as a function of monthly median mixed layer light intensities, which results in the expression

$$(Chl/\mathrm{C})_{\mathrm{N\text{-}Tmax}} = \left[0.022 + (0.045 - 0.022)e^{-3Ig}\right] \tag{8}$$

The above expression is a representation of *Chl*:C in nutrient-replete, optimal growth conditions, e.g., the maximum potential *Chl*:C for a given irradiance. The two constants in the above equation reflect a low-light maximum in *Chl*:C (0.045 mg *Chl*/mg C) and a high-light asymptotic value (0.022 mg *Chl*/mg C).

Ig (model-photons m^{-2} d^{-1} h^{-1}) is the median mixed layer light level, obtained using SeaWiFS PAR and K_{490}, and the spectral fractionation numerical method [*Austin and Petzold*, 1986; *Voss*, 1992]

$$Ig = \frac{1}{dl} \int E_{Zmld}(\lambda)\, d\lambda \tag{9}$$

where E_{Zmld} is the spectral median mixed layer light level in moles-photons m^{-2} d^{-1} nm^{-1} given by

$$E_{Zmld}(\lambda) = 0.975 E_{\mathrm{o}}(\lambda) e^{(-K_d(\lambda)\frac{MLD}{2})} \tag{10}$$

The surface spectral PAR $E_o(\lambda)$, in moles-photons m^{-2} d^{-1} nm^{-1}, is obtained from the following equations that fractionate the integrated surface PAR into nine band components using the spectral coefficients $f(\lambda)$ in nm^{-1}

$$\begin{aligned} &E_{\mathrm{o}}(\lambda) = f(\lambda)\mathrm{PAR} \\ &f(\lambda) = [0.0029,\ 0.0032,\ 0.0035,\ 0.0037,\ 0.0037,\ 0.0036,\ 0.0032,\ 0.0030,\ 0.0024] \\ &\lambda(\mathrm{nm}) = [400,\ 412,\ 443,\ 490,\ 510,\ 555,\ 625,\ 670,\ 700] \end{aligned} \tag{11}$$

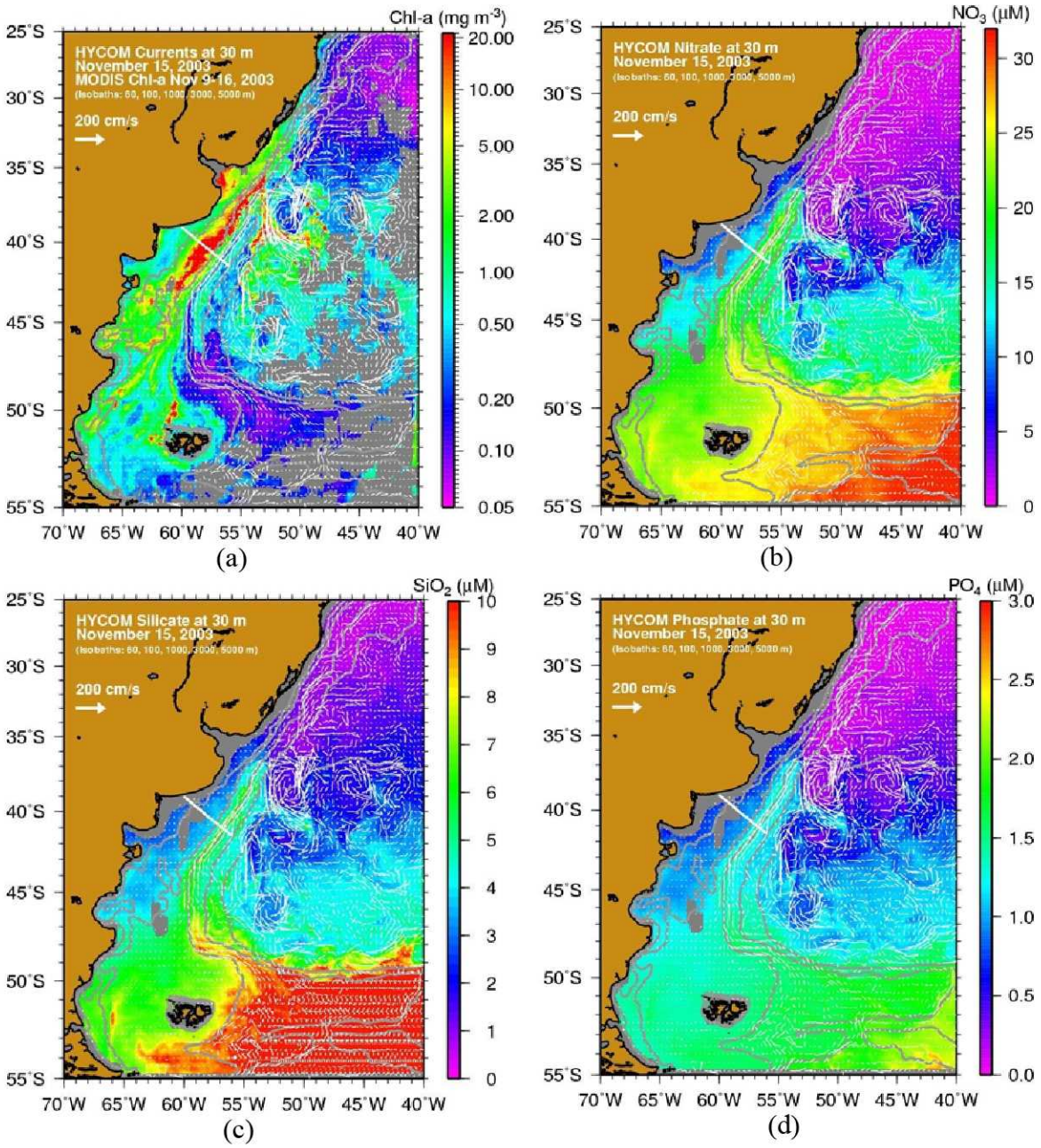

Figure 12. Eight-day composite of MODIS *Chl-a* for November 9-16, 2003 (a), and HYCOM-derived nitrate (b), silicate (c), and phosphate (d) for November 15, 2003. HYCOM currents (white vectors) for November 15, 2003 are plotted over each image.

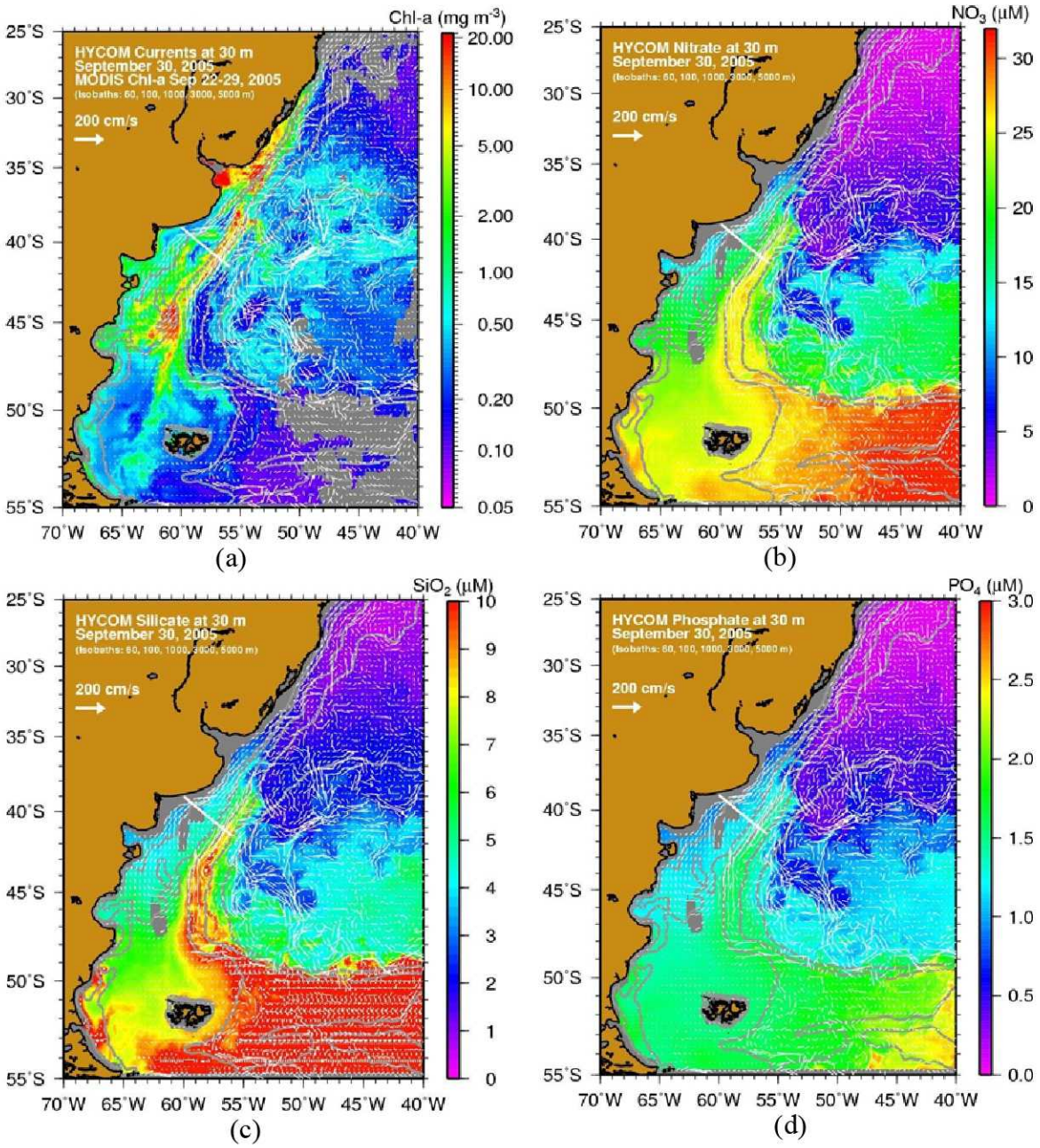

Figure 13. Eight-day composite of MODIS *Chl-a* for September 22-29, 2005 (a), and HYCOM-derived nitrate (b), silicate (c), and phosphate (d) for September 30, 2005. HYCOM currents (white vectors) for September 30, 2005 are plotted over each image.

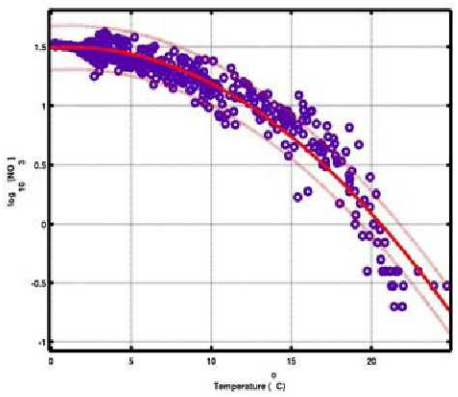

(a)

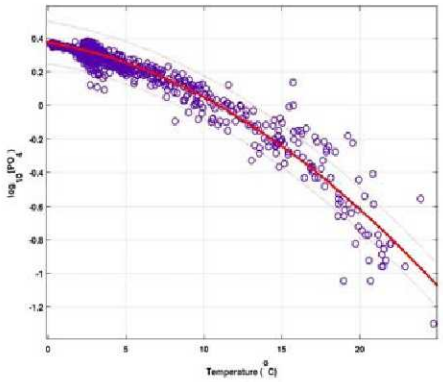

(b)

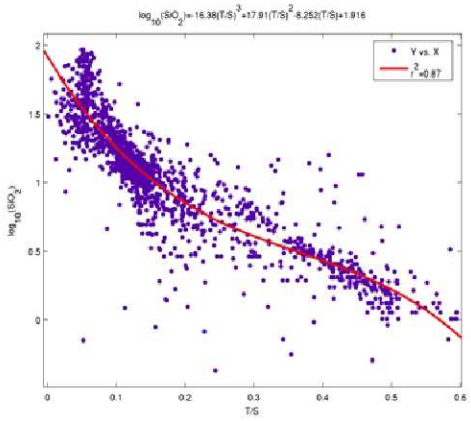

(c)

Figure 14. (a) Regression of nitrate versus temperature: $\log_{10}[NO_3]$=-0.003999*T^2 + 0.009936*T + 1.488. (b) Regression of phosphate versus temperature: $\log_{10}[PO_4]$=-0.0002051*T^3 + 0.003571*T^2 - 0.05464*T + 0.4319. (c) Regression of silicate versus T/S: $\log_{10}[SiO_3]$=-16.38*$(T/S)^3$ + 17.91*$(T/S)^2$ – 8.252*T + 1.916, r^2=0.87.

The spectral diffuse attenuation, $K_d(\lambda)$ in m^{-1}, as a function of K_{490} and the spectral diffuse attenuation for water K_{dw}, is given by

$$K_d(\lambda) = \frac{M(\lambda)}{M(490)}\left[K_{490} - K_{dw}(490)\right] + K_{dw}(\lambda) \quad (12)$$

$M(\lambda)$ and K_{dw} (λ) are tabulated constants, interpolated to the 9 discrete wavelengths from the multi-spectral values given in *Austin and Petzold* [1986]. The day length *dl* (in hours) is obtained from a function of year-day and latitude. The input parameters are for the period of November 7, 2003 – September 7, 2007 at 8-day resolution and averaged within the shelf domain delimited by the 5 mg/m^3 *Chl-a* contour obtained from the SeaWiFS *Chl-a* December 2003 composite. The input data originate from SeaWiFS GSM *Chl-a* ($mgChl/m^3$) and b_{bp} (in m^{-1}) 8-day composites, SeaWiFS PAR (moles-photons/m^2/d) and K_{490} (m^{-1}) 8-day composites, and HYCOM daily temperature and salinity to derived nutrient concentrations, and HYCOM mixed layer thickness, together with PAR and K_{490}, to calculate E_{zmld}.

Figure 17 shows the time series of GSM *Chl-a*, HYCOM mixed layer depth, and satellite-derived growth, carbon biomass, and net primary production (NPP) averaged within the shelf domain defined above. Although there is some interannual variability in the growth, the variability does not correlate with the large carbon biomass observed during the anomalous bloom. If we assume that the satellite-derived growth is accurate and captures the underlying changes in nutrient availability, then the explanation for the large biomass observed in 2003 must be elsewhere (grazer pressure, different proportion of functional groups, other physiological explanation?). One limitation of this method is that there is no distinction of functional groups and no explicit assessment of iron limitation effects, which we attempt to address in the next section.

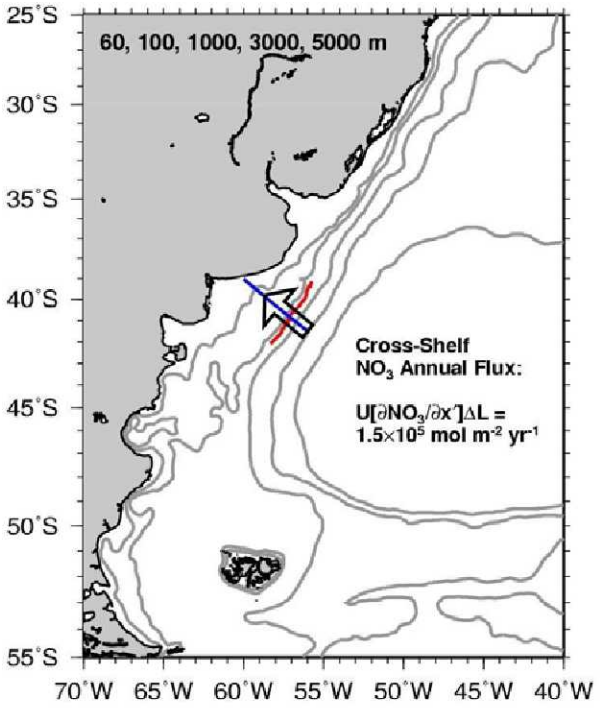

Figure 15. Map showing the along-shelf transect (red line) at which the on-shelf nitrate flux (large black arrow) time series was calculated. The annual averaged nitrate flux was 1.5×10^5 mol NO_3 m^{-2} yr^{-1}. The blue line indicates the cross-shelf transect through the middle of the shelf bloom.

3.6.3 Growth of Diatoms and Small Phytoplankton Based on Analytical Approach and Numerical Model Results

Using *Chl-a*, SST, and nutrients from model simulations (*Chl-a*, SST, NO_3, PO_4, SiO_3, dissolved iron DFe, and NH_4), together with analytical equations relating nutrient concentration and euphotic zone light penetration to growth, an estimate of growth for diatoms and small phytoplankton was obtained for the study region. Monthly climatologic surface nutrients, chlorophyll and temperature originate from the global ocean Biogeochemical Elemental Cycling (BEC) ocean model of *Moore and Braucher* [2008]. This is a global three-dimensional marine ecosystem model with several key phytoplankton functional groups, multiple limiting nutrients, explicit iron cycling, and a mineral ballast/organic matter parameterization. The model is run within a global circulation model. The model grid (102×116 grid points) has a longitudinal resolution of 3.6° longitude, and a latitudinal resolution which varies from 1° to 2°, with higher resolution near the equator. The caveat is that in the southwest Atlantic the model does not perform really well. The bloom in that region tends to be too big, and the coarse resolution doesn't capture the Malvinas Current well. Therefore, since the model does not resolve finer scale features, such as the Malvinas upwelling zone along the shelf break, an interpolation scheme was developed which uses the coarser resolution model products within the upper 40 meters to derive nutrient distributions based on higher resolution satellite images of *Chl-a* and SST. Figures 18 through 24 show monthly maps of *Chl-a*, Fe, NO_3, SiO_3, PO_4, and NH_4, respectively, subset for the region of interest. These model results were used to derive nutrient regressions. The results are shown in equations 13 and 14 and the coefficients are given in Table 1.

$$\log_{10}(X) = c_0 + c_1 T + c_2 T^2 + c_3 \log_{10}(Chl) + c_4 T \log_{10}(Chl) + c_5 [\log_{10}(Chl)]^2 \quad (13)$$

$$\log_{10}(\mathrm{Fe}) = d_0 + d_1 Mo + d_2 Mo^2 + d_3 Lon + d_4 Lat + d_5 T + d_6 T^2 + d_7 \log_{10}(Chl) + d_8 \left[\log_{10}(Chl)\right]^2 \quad (14)$$

Figures 25 and 26 show the 8-day composite images of MODIS Aqua *Chl-a*, and the derived nutrients (DFe, NO_3, and SiO_3) from satellite SST and *Chl-a* for two time periods, December 11-18, 2003, and September 22-29, 2005. These two periods highlight extreme high and extremely low biomass on the Patagonian shelf during spring. Note in these figures that the southern portion of the region, where the MC originates, the macro nutrients concentrations are relatively elevated while DFe concentrations are the lowest in the region. The shelf region, however, shows higher DFe and

macro nutrient concentrations, while the subtropical gyre region is poor in macro nutrients but relatively rich in DFe. This scenario is consistent with the satellite-derived biomass distribution.

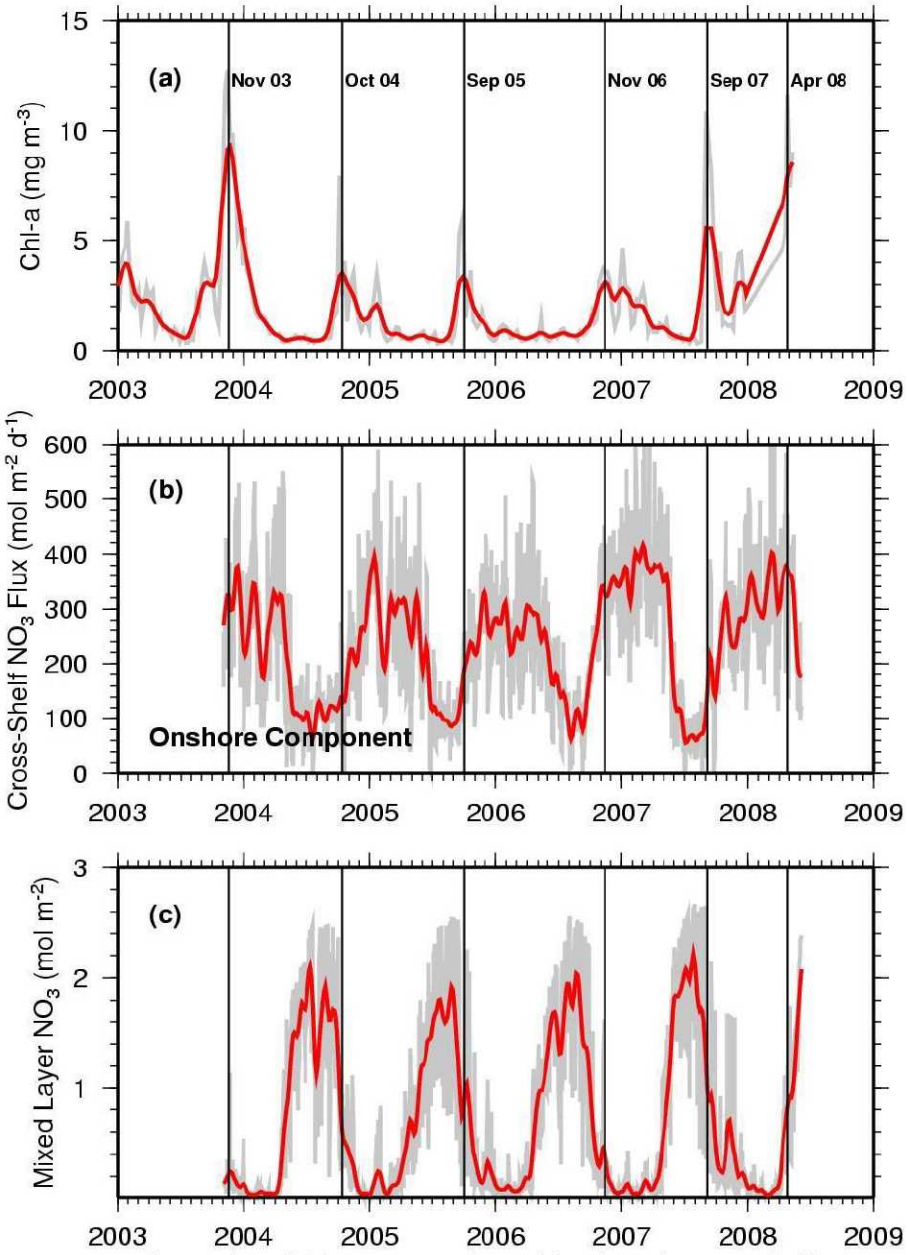

Figure 16. Time series of (a) mean SeaWiFS *Chl-a* along the cross-shelf transect (blue line in Figure 1), (b) onshore component of nitrate flux, and (c) mean mixed layer nitrate along the cross-shelf transect. The grey line in (a) is the 8-day *Chl-a*, while the red line is the low-pass filtered data. The same applies for (b) and (c), except that the grey lines represent daily data. The vertical lines are markers for the peak *Chl-a* concentration.

The growth equations for diatoms (DA) and small phytoplankton (SP) can be written as [*Signorini and McClain*, 2003]:

$$\begin{aligned} \mu\mathrm{DA} &= F_{phy}(E)\,\min\left[\mathrm{N_{lim}}, \mathrm{PO_{4lim}}, \mathrm{SiO_{3lim}}, \mathrm{Fe_{lim}}\right] \\ \mu\mathrm{SP} &= F_{phy}(E)\,\min\left[\mathrm{N_{lim}}, \mathrm{PO_{4lim}}, \mathrm{Fe_{lim}}\right] \end{aligned} \tag{15}$$

Table 1. Coefficient values for nutrient polynomial regressions (equations 13 and 14) based on BEC ocean model.

X	c_o	c_1	c_2	c_3	c_4	c_5				r^2
NO_3	2.056	-0.175	-0.863	0.00435	0.101	-0.530	-	-	-	0.73
SiO_3	2.127	-0.09008	0.198	-0.00176	-0.0353	0.03759	-	-	-	0.84
PO_4	-0.155	0.09624	-0.886	-0.0086	0.08475	-0.350	-	-	-	0.86
NH_4	-0.604	0.03512	-0.470	-0.0063	-0.02017	-0.639	-	-	-	0.65
	d_0	d_1	d_2	d_3	d_4	d_5	d_6	d_7	d_8	r^2
Fe	-1.369	0.222	-0.01389	-0.01936	0.02904	0.08857	-0.00426	-0.201	-0.01051	0.52

The light-dependent function is $F_{phy}(E) = \mu_{\max}\alpha E / \left[\mu_{\max}^2 + (\alpha E)^2\right]$, where μ_{max}=3.0 d^{-1} is the maximum phytoplankton growth, α=0.25 $(Wm^{-2})^{-1}$ d^{-1} is the slope of the P-I curve, and E is the PAR at depth z in W m^{-2}.

The nutrient limitation functions for nitrogen, phosphate, silicate, and iron are

$$\begin{aligned} \mathrm{N_{lim}} &= \mathrm{NH_{4lim}} + \mathrm{NO_{3lim}} \\ \mathrm{NH_{4lim}} &= \frac{\mathrm{NH_4}}{\left(\mathrm{NH_4} + K_{\mathrm{NH}}\right)} \\ \mathrm{NO_{3lim}} &= \frac{\mathrm{NO_3}}{\left(\mathrm{NO_3} + K_{\mathrm{N}}\right)}\left[1 - \mathrm{NH_{4lim}}\right] \\ \mathrm{PO_{4lim}} &= \frac{\mathrm{PO_4}}{\left(\mathrm{PO_4} + K_{\mathrm{P}}\right)} \\ \mathrm{SiO_{3lim}} &= \frac{\mathrm{SiO_3}}{\left(\mathrm{SiO_3} + K_{\mathrm{S}}\right)} \\ \mathrm{Fe_{lim}} &= \frac{\mathrm{DFe}}{\left(\mathrm{DFe} + K_{\mathrm{F}}\right)} \end{aligned} \tag{16}$$

where, K_N, K_{NH}, K_P, Ks, and K_F are the half-saturation constants for nitrate, ammonium, phosphate, silicate, and iron, respectively. Following *Lancelot et al*. [2000], we used the values K_N =1.0 µM, K_P =0.2 µM, and K_F =1.2 nM for southern ocean diatoms. Ks was set to 1.0 µM for diatoms only and K_F =0.12 nM for small phytoplankton. *Timmermans et al.* [2004] conducted growth experiments with four large open ocean diatoms from the Southern Ocean in natural (low iron) Southern Ocean seawater with increasing Fe concentrations. Their results showed that growth rates increased three- to six-fold with increasing DFe, and the species with the smallest cells had the highest growth rates. They report Fe half-saturation constants (K_F) for growth ranging from 0.19 to 1.14 nM.

The averaged euphotic zone PAR, $E(Ze)$, was analytically derived from the integral of the light attenuation exponential function

$$E(Z_{eu}) = \frac{E_o}{Z_{eu} K_{\mathrm{PAR}}} \left[1 - e^{-K_{\mathrm{PAR}} Z_{eu}} \right], \text{ where } Eo \text{ is the surface PAR} \qquad (17)$$

From *Morel* [1988], Z_{eu} and the mean K_{PAR} within Z_{eu} can be evaluated from *Chl* as

$$\begin{aligned} Z_{eu} &= 38.0 Chl^{-0.428} \\ K_{\mathrm{PAR}} &= 0.121 Chl^{0.428} \end{aligned} \qquad (18)$$

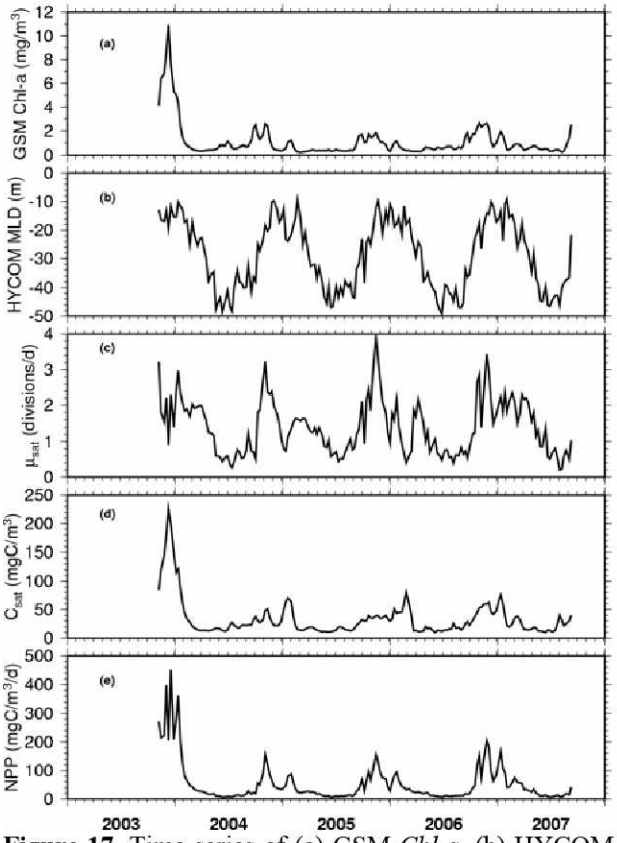

Figure 17. Time series of (a) GSM *Chl-a*, (b) HYCOM mixed layer depth, (c) satellite-derived growth using CbPM, (d) satellite-derived phytoplankton carbon using CbPM, (e) satellite-derived net primary production in the mixed layer ($\mu_{sat} \times C_{sat}$).

Figure 27 shows time series of MODIS Aqua *Chl-a* and SST, derived DFe and macro nutrients (NO_3, SiO_3, PO_4, NH_4), and the analytical diatom and small phytoplankton growths. The vertical lines in Figure 17 mark the peak *Chl-a* concentrations on the series. Note that the diatom growth is always smaller (about ½) than the small phytoplankton growth. The *Chl-a* concentration peaks near maximum E_{Ze} and shallowest MLD. The *Chl-a* concentration begins to rise when DFe is at its maximum concentration, the MLD is deepest, and E_{Ze} begins to increase. The maximum growth of diatoms and small phytoplankton occurs almost always during the maximum *Chl-a* concentration. Table 2 tabulates *Chl-a*, SST, nutrient, and growth values for the periods during which *Chl-a* concentration reached a maximum value. The lowest concentration of all nutrients occurs around the middle of December 2003 when *Chl-a* attained the highest concentrations (~25 mg m^{-3}) of the entire time series.

Eight-day images of spatial distribution of diatom and small phytoplankton growth are shown in Figure 28 for December 11-18, 2003, and September 22-29, 2005. HYCOM surface currents for the same periods are superposed and seem to provide good agreement with the spatial distribution of phytoplankton growth, and thus biomass.

Table 2. Biogeochemical parameter values at the occasion of the *Chl-a* peak (see Figure 27). Tabulated parameters are MODIS *Chl-a* (mg m^{-3}), MODIS SST (°C), derived near-surface (Z_{pd}) dissolved iron (DFe in nM), derived surface nitrate (NO_3 in µM), silicate (SiO_3 in µM), phosphate (PO_4 µM)), ammonium (NH_4 µM), and diatoms (µDA) and small phytoplankton (µSP) growths from analytical formulation. The last column tabulates the averaged PAR within the euphotic layer.

Date	*Chl-a*	SST	DFe	NO_3	SiO_3	PO_4	NH_4	µDA	µSP	E_{PAR}
11/20/2002	7.1	12.6	0.47	3.17	4.41	0.41	0.020	0.56	1.29	27.3
12/14/2003	24.5	14.0	0.27	2.00	1.91	0.21	0.001	0.38	1.00	28.1
9/25/2004	5.0	9.4	0.67	5.34	14.64	0.72	0.090	0.49	1.01	16.1
9/25/2005	3.2	9.8	0.75	4.59	12.87	0.72	0.102	0.54	1.07	16.3
11/12/2006	5.7	12.2	0.52	3.60	5.70	0.48	0.035	0.55	1.25	24.2
12/14/2007	6.7	13.6	0.39	3.27	3.24	0.36	0.021	0.48	1.23	27.5

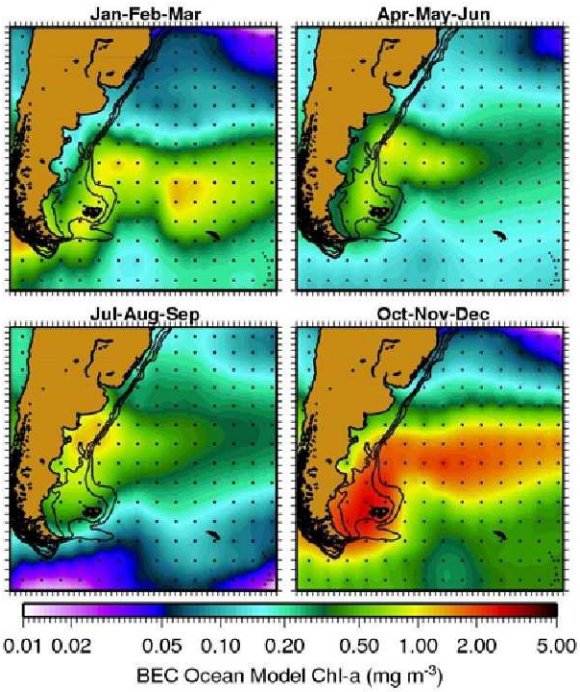

Figure 18. Seasonal maps of top-layer (Z_{pd}) chlorophyll re-gridded at 0.5°×0.5° resolution from the Biogeochemical Elemental Cycling (BEC) ocean model [*Moore and Braucher*, 2008].

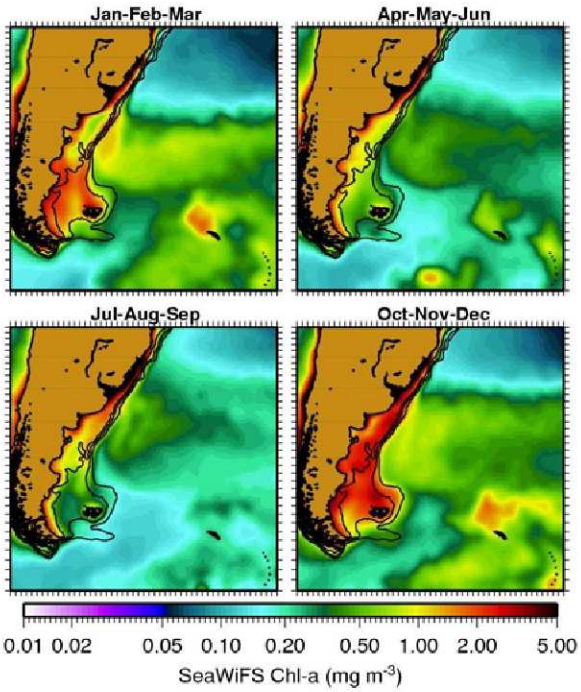

Figure 19. Seasonal maps of SeaWiFS chlorophyll. Compare with BEC chlorophyll maps in Figure 18.

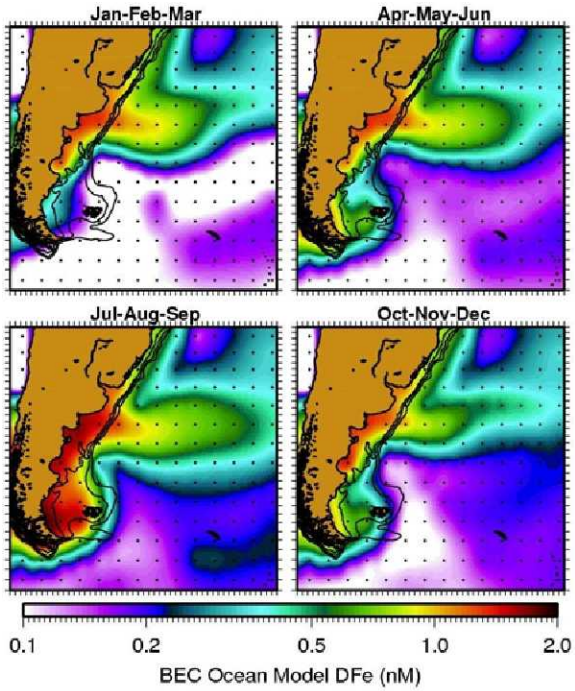

Figure 20. Seasonal maps of top-layer (Z_{pd}) dissolved iron (DFe) re-gridded at 0.5°×0.5° resolution from the Biogeochemical Elemental Cycling (BEC) ocean model [*Moore and Braucher*, 2008].

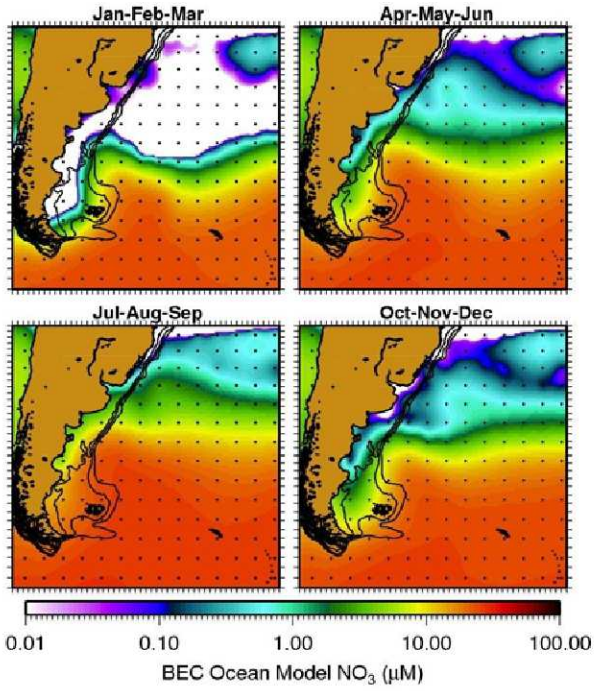

Figure 21. Seasonal maps of top-layer (Z_{pd}) nitrate (NO_3) re-gridded at 0.5°×0.5° resolution from the Biogeochemical Elemental Cycling (BEC) ocean model [*Moore and Braucher*, 2008].

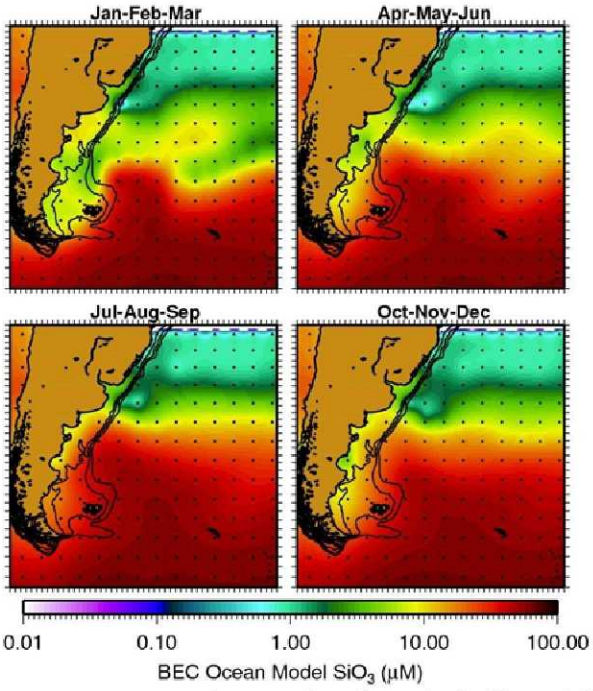

Figure 22. Seasonal maps of top-layer (Z_{pd}) silicate (SiO_3) re-gridded at 0.5°×0.5° resolution from the Biogeochemical Elemental Cycling (BEC) ocean model [*Moore and Braucher*, 2008].

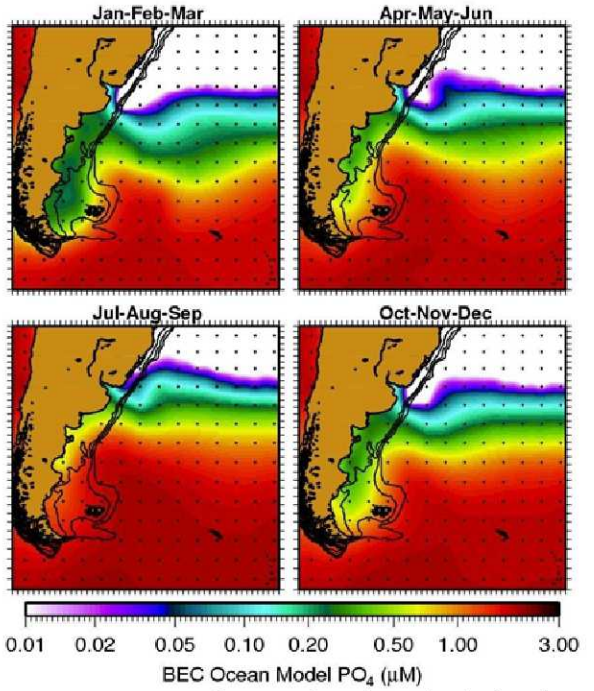

Figure 23. Seasonal maps of top-layer (Z_{pd}) phosphate (PO_4) re-gridded at 0.5°×0.5° resolution from the Biogeochemical Elemental Cycling (BEC) ocean model [*Moore and Braucher*, 2008].

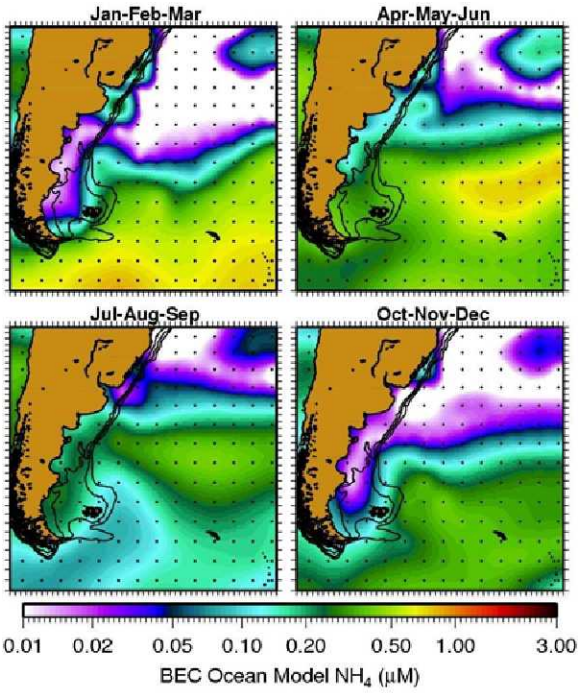

Figure 24. Seasonal maps of top-layer (Z_{pd}) ammonium (NH_4) re-gridded at 0.5°×0.5° resolution from the Biogeochemical Elemental Cycling (BEC) ocean model [*Moore and Braucher*, 2008].

Note from the growth maps that diatoms should be more abundant on the shelf and along the subtropical convergence where there are indications from this analysis that DFe concentrations are higher. Small phytoplankton growth is more widespread in the open ocean as they require less DFe to grow, but seems to be stronger along the shelf and shelf break in general. In addition, both DA and SP growths are much higher during December 2003 than September 2005.

3.6.4 High Resolution, Empirically Derived Seasonal Surface Nutrient Climatology

Seasonal composites of MODIS Chl-a and SST are shown in Figure 29. Monthly composites of MODIS Chl-a and SST, combined with empirical equations 13 and 14, were used to calculate 9-km monthly surface nutrient distributions. The monthly surface nutrient fields were then binned to produce seasonal (quarterly) composites. Daily HYCOM surface vector currents, from the period of November 2003 − July 2008, were averaged into seasonal composites and superposed on all the seasonal maps. Seasonal maps of nitrate, dissolved iron, silicate, and phosphate are shown in Figures 30 and 31. These empirical estimates are based on regressions using the coarse resolution BEC model [*Moore and Braucher*, 2008] simulations (see Figures 20 through 23) and therefore do not accurately capture nearshore sources of nutrients, such as the Rio de La Plata plume and the discharge from the Patos and Mirim lagoon system (~30°S to ~37°S along the coast). The Rio de La Plata plume is known to be a significant source of silicate [*Ciotti et al.*, 1995], and there are field studies showing that the lagoons are a significant source of iron enriched submarine groundwater that seeps through sediment in the nearshore region [*Niencheski et al.*, 2007; *Windom et al.*, 2006]. However, the BEC ocean model includes sedimentary and mineral dust sources of dissolved iron. The sedimentary Fe source is incorporated as a constant flux of 2 µmol Fe m^{-2} d^{-1} from sediments at the bottom of the ocean grid whenever depth is less than 1100 m. Dust deposition is from the climatology of *Luo et al.* [2003]. The model has recently been applied to quantify ocean biogeochemical sensitivity to variations in mineral dust deposition (iron inputs) [*Moore et al.*, 2006], the feedbacks between denitrification and nitrogen fixation [*Moore and Doney*, 2007], and the ocean biogeochemical response to atmospheric deposition of inorganic nitrogen [*Krishnamurthy et al.*, 2007].

A close examination of Figures 30 and 31 reveals that the Malvinas Current transports high concentrations of nitrate, silicate, and phosphate northward along the Patagonian shelf break. However, these same southern waters are depleted in iron, as shown by the empirically derived seasonal maps of DFe in Figure 30 (right panel). This is consistent with the low Chl-a concentrations observed by ocean color satellites, as shown by the MODIS seasonal composites in Figure 29 (left panel). Dissolved iron concentrations in surface waters reach a maximum on the Patagonian shelf

waters in winter, as shown by the July-August-September composite in Figure 30, most likely a result of intensified water column iron sediment flux via vigorous mixing by storms and convective overturning. By summer (January-February-March composite in Figure 30), the surface iron is significantly depleted as a result of uptake during the spring bloom.

4. Summary and Conclusions

This study reveals that the Patagonian shelf and shelf break regions are characterized by significant interannual variability of phytoplankton productivity. The intensity and geographic extent of the phytoplankton blooms are well documented by ocean color satellites but the mechanisms that drive the large interannual variability are not entirely understood. The anomalous 2003 bloom discussed in this paper is a clear example of how large the year-to-year changes can be. These large changes in phytoplankton productivity must be associated with corresponding changes of nutrient supply but its sources are not entirely known. In particular, the soluble Fe sources are still elusive despite a large body of literature that identifies riverborne, airborne, and oceanic sources of bioavailable Fe controlling biological activity in this region.

Regarding airborne sources, it is possible to identify potential atmospheric factors controlling iron delivery to the South Atlantic and possible association with Chl-a blooms: (1) the climatic regime (aridity level) of the Patagonian semi-arid desert that would impose differential dust emissions to the Southern Atlantic Ocean, both in yearly and in long-term time scales, as retrieved from ice-cores from Antarctica; (2) episodic volcanic contribution that may act in two ways: as a source of soluble iron and as an indirect factor, through the SO_2 supply that would promote solubilization of atmospheric iron blown from the desert surface; and, (3) integrated contribution of several industrialized sites of South America with population higher than 6 million habitants (Rio de Janeiro, São Paulo, Buenos Aires, Santiago and Lima), with sulfur emissions underestimated by current inventories.

It is important to determine Fe fluxes and concentrations in this important biologically active region, as well as the overall balance of macro and micro nutrients that control the phytoplankton seasonal and interannual variability. The MC upwelling along the PSB has been previously identified as a major source of macronutrients but Fe has not been measured in the MC waters to unequivocally explain the PSB spring-summer bloom biogeochemical dynamics. However, interannual changes in the summer MLD modulate the intensity and transition of functional groups on the shelf and PSB bloom regions and episodic MC intrusions (deflections) fertilize the shelf region with nutrient-rich waters. Also, the mechanisms that drive the timing of the PSB spring bloom can be explained using the Sverdrup critical depth theory.

The core of the Malvinas Current (MC) is a conduit of macro-nutrient-rich waters originating in the southernmost region of the study domain. However, the MC core has low phytoplankton biomass compared with the Patagonian shelf and shelf break regions. Although dissolved iron (DFe) concentration observations are still scarce in this region, the abundance of macro-nutrients and low *Chl-a* concentrations in the MC core could be an indication of depleted DFe waters. Alternatively, much higher concentrations of *Chl-a* on the shelf seem to indicate the presence of waters with more abundant DFe. Model simulations [*Moore and Braucher*, 2008; *Moore et al.*, 2002a; *Moore et al.*, 2002b; *Moore et al.*, 2004] combined with a global compilation of DFe observations, predict column-integrated inputs of DFe iron fluxes from mineral dust (0.3-0.6 mmol Fe/m^2/yr) and sediments (0.6-1.0 mmol Fe/m^2/yr) in the Patagonian shelf region that are high relative to other global ocean regions.

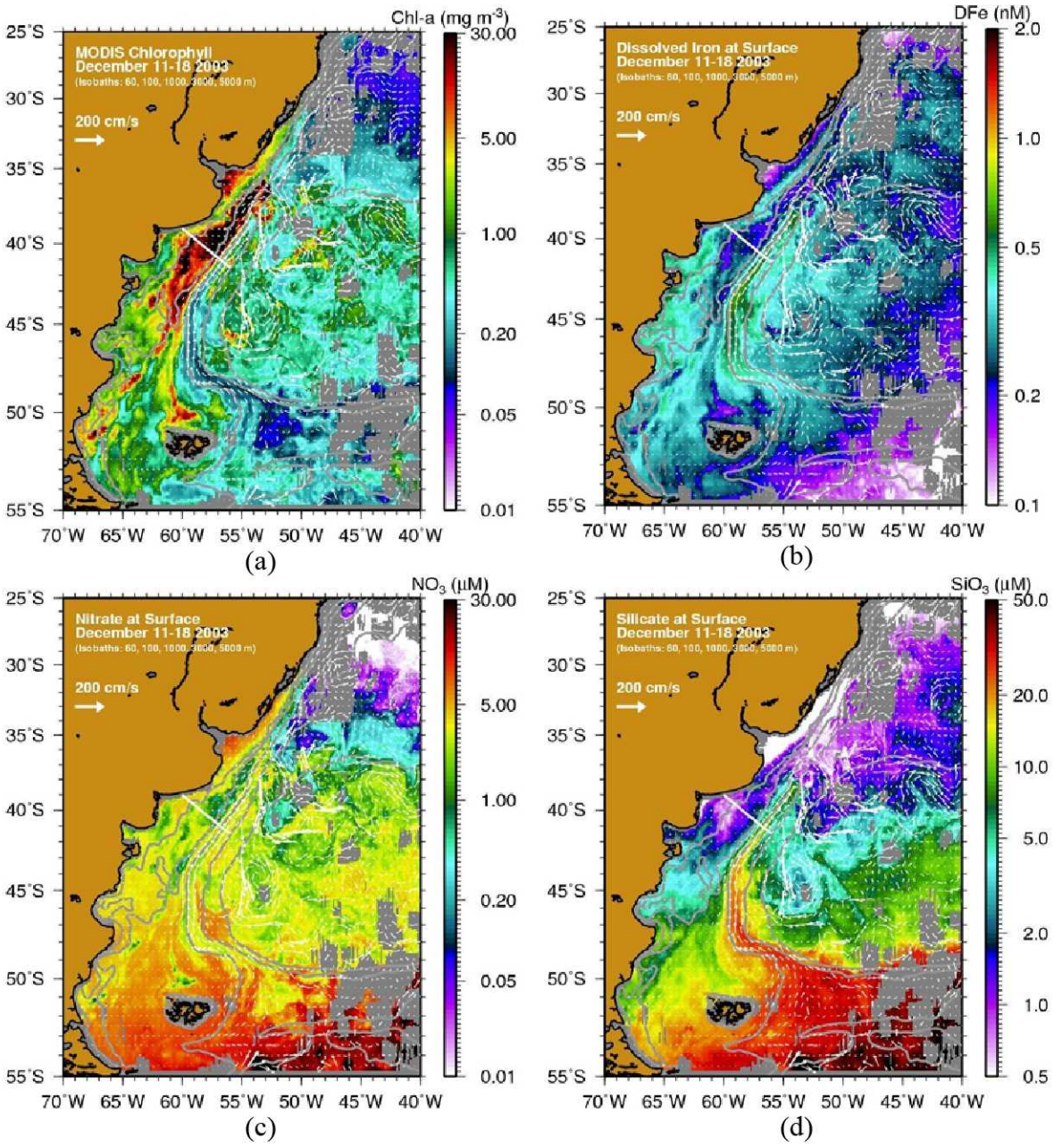

Figure 25. MODIS *Chl-a* (a), and derived near-surface (Z_{pd}) dissolved iron (b), nitrate (c), and silicate (d) for December 11-18, 2003.

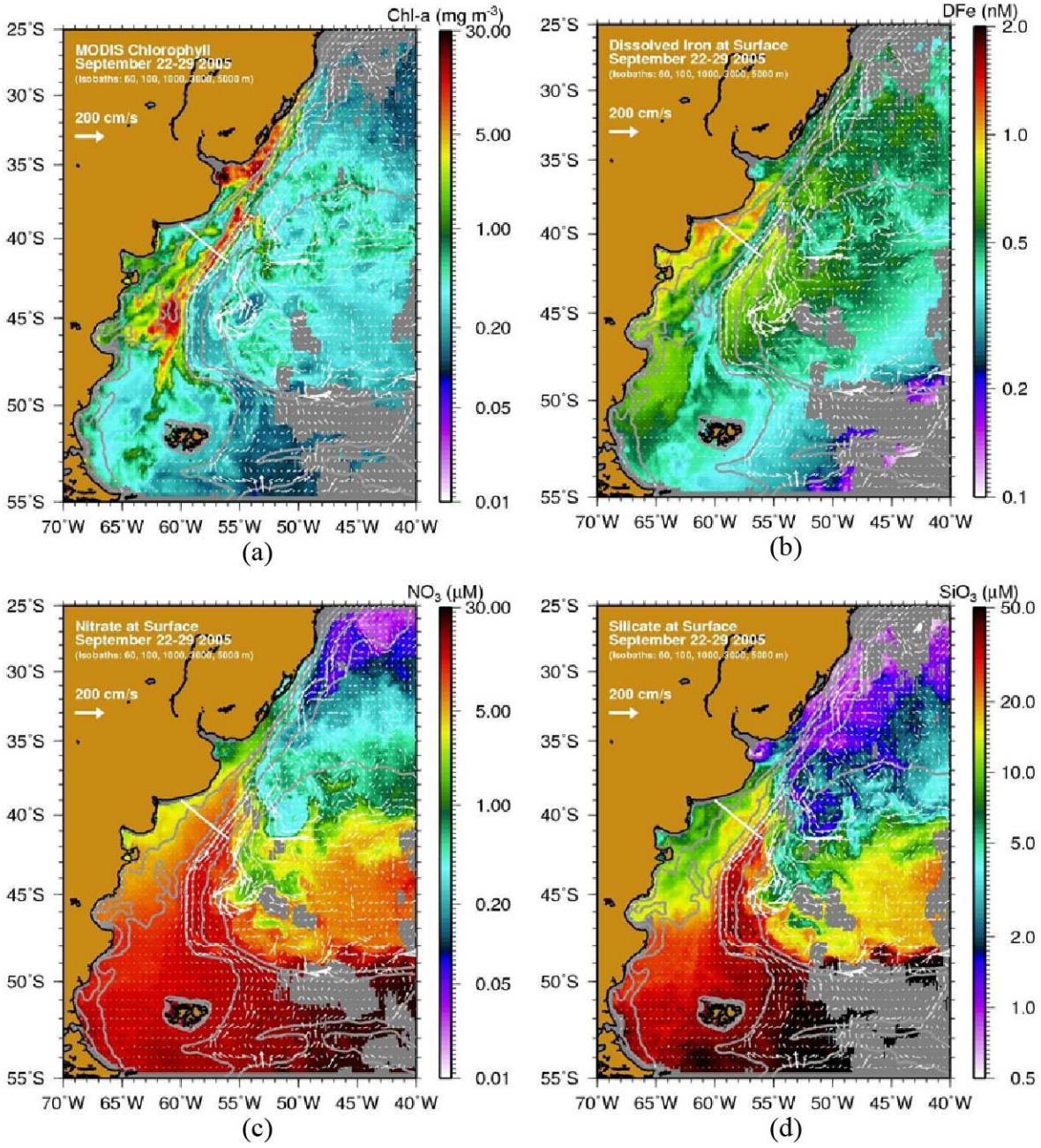

Figure 26. MODIS *Chl-a* (a), and derived near-surface (Z_{pd}) dissolved iron (b), nitrate (c), and silicate (d) for September 22-29, 2005.

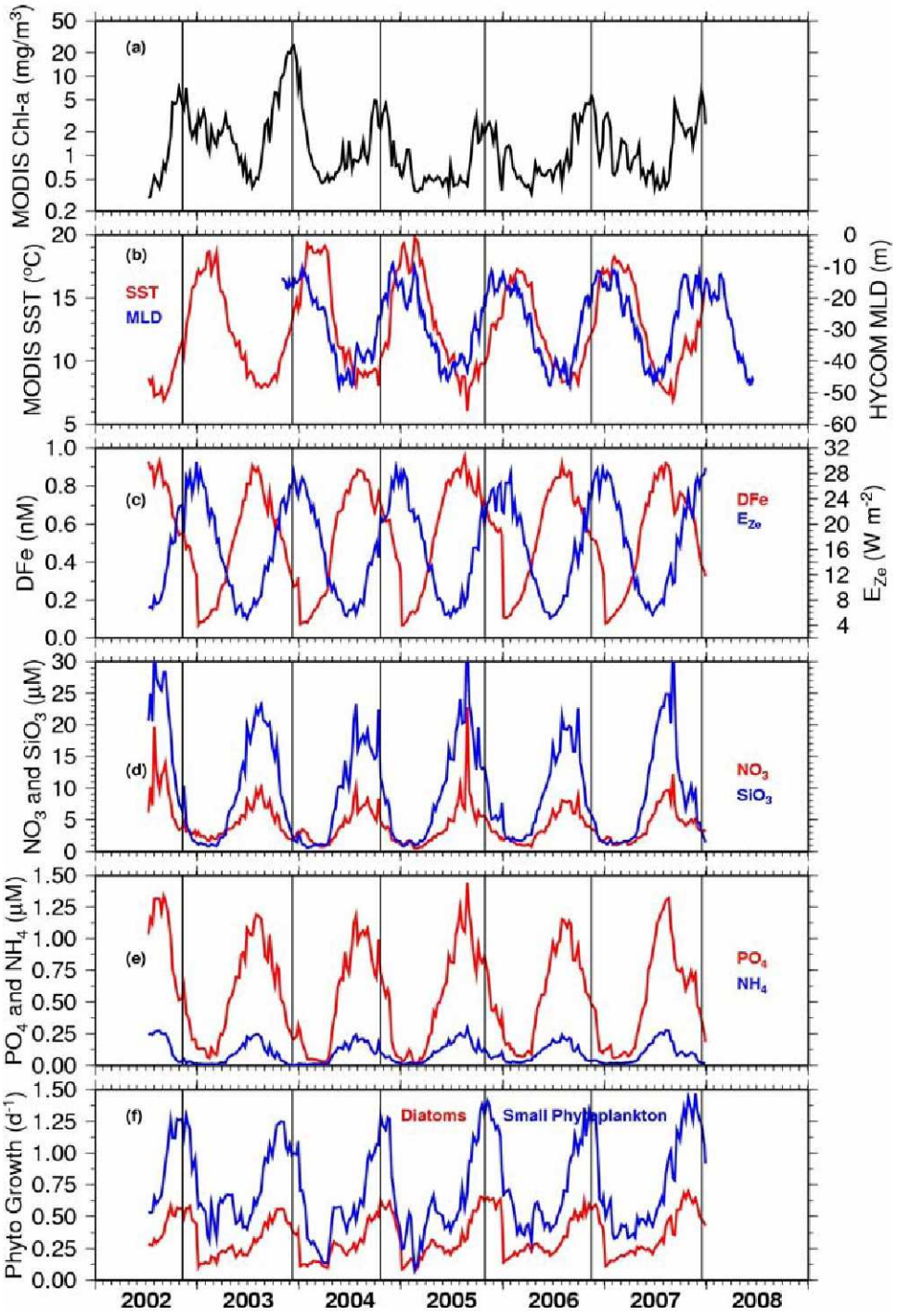

Figure 27. Time series of (a) MODIS *Chl-a*, (b) MODIS SST and HYCOM mixed layer depth (MLD), (c) derived dissolved iron (DFe) and mean euphotic depth PAR (E_{Ze}), (d) surface derived nitrate and silicate, (e) phosphate and ammonium, and (f) modeled diatom and small phytoplankton growth. All parameters were averaged within the 5 mg m^{-3} *Chl-a* contour obtained from the December 2003 composite on the shelf. The vertical lines are markers for the peak *Chl-a* concentration.

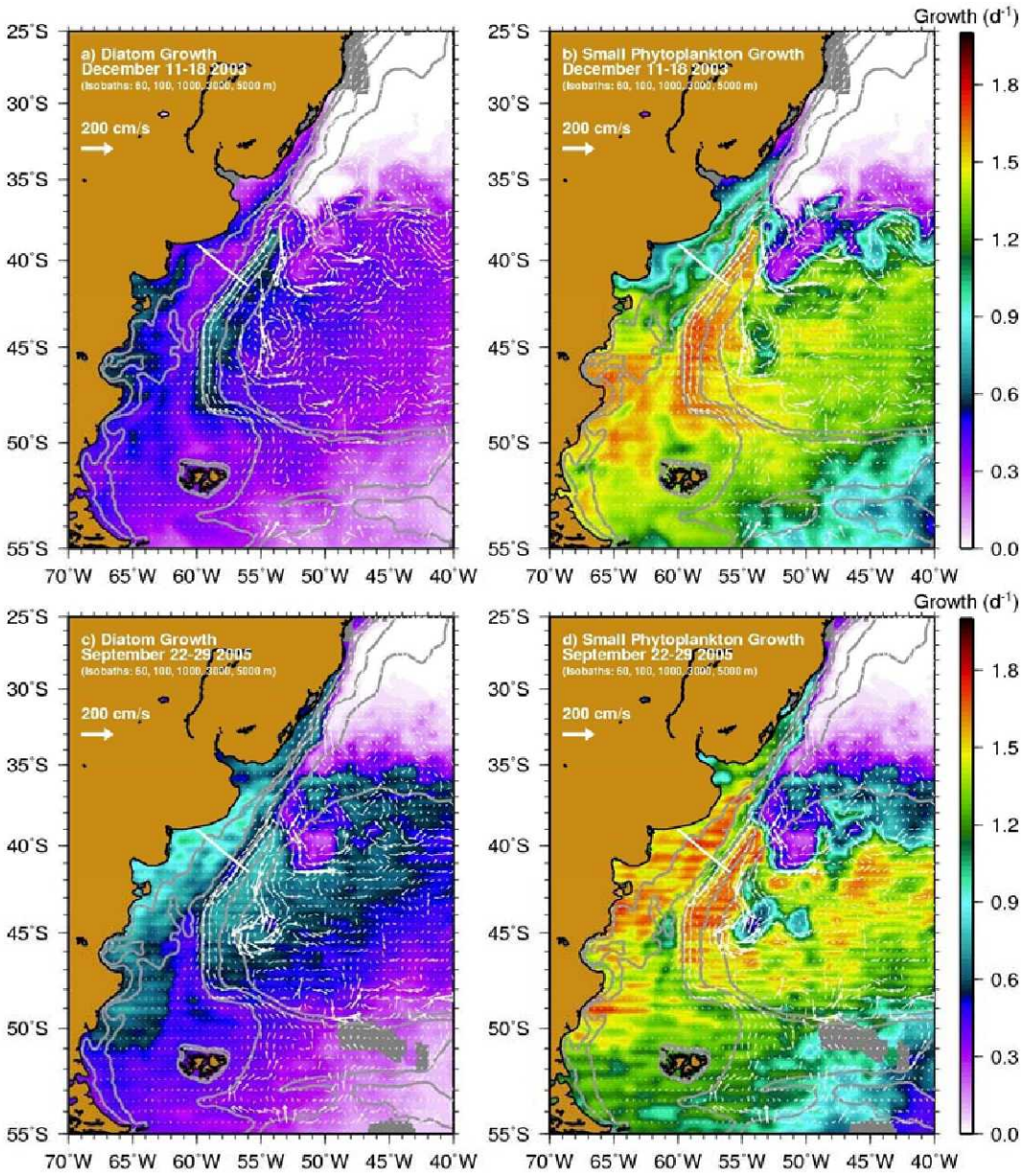

Figure 28. Near-surface (Z_{pd}), eight-day maps of diatom and small phytoplankton growth for December 11-18 2003 (*a* and *b*) and September 22-29 2005. HYCOM surface currents for the same time period are superposed.

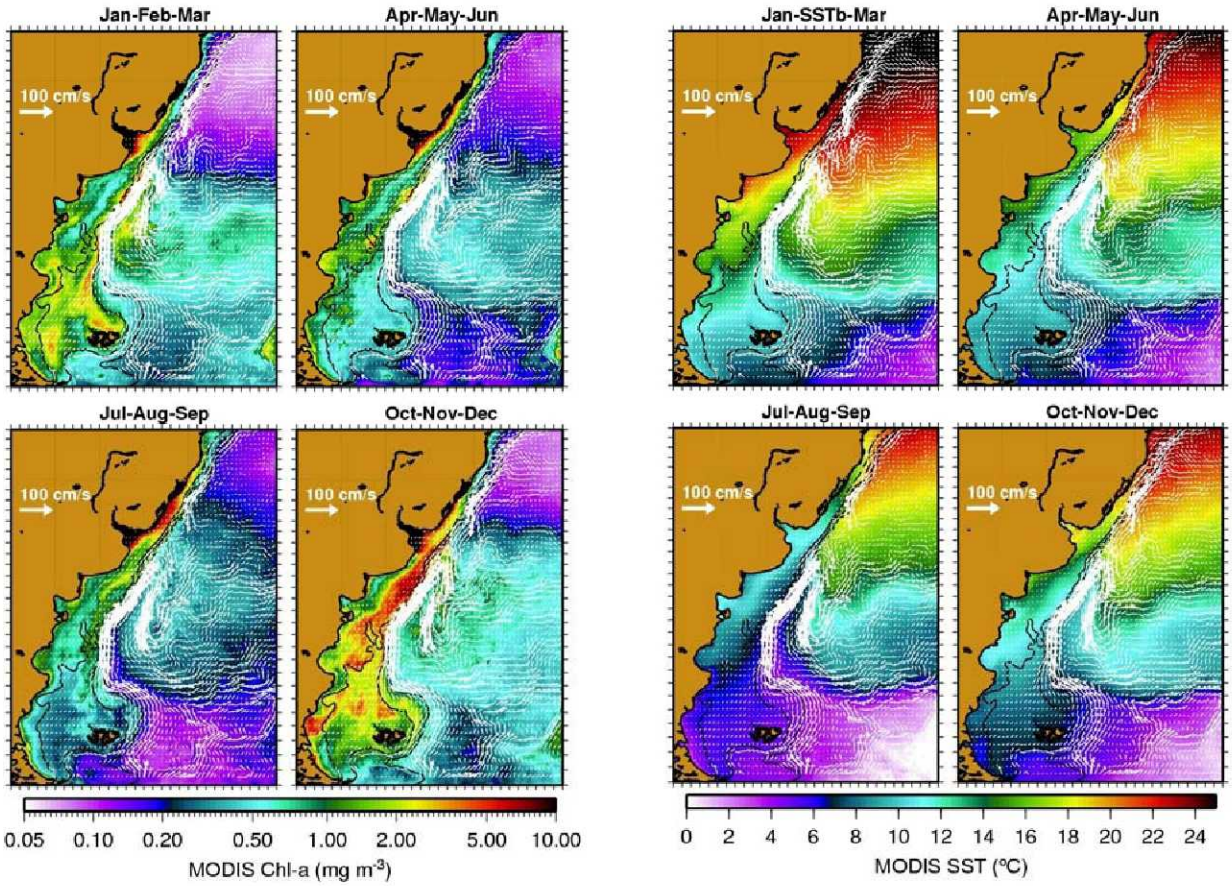

Figure 29. Seasonal composites of MODIS Chl-a (left panel) and SST (right panel). The white vectors represent seasonal HYCOM surface currents.

Although this analysis provided further insights in the relationship between biomass and nutrient cycling, the driving mechanisms and DFe sources for the extremely elevated biomass on the Patagonian shelf region during the spring of 2003 remain elusive. Further investigations, including comprehensive field data collection and numerical modeling, with emphasis on iron sources and nutrient concentrations, will be indispensable to unravel the large interannual changes in biomass seen by ocean color satellites in the region. There are existing three dimensional, coupled physical-biogeochemical models for applications in continental shelf systems that can be configured for the Patagonian shelf region. One example is the Regional Ocean Modeling System (ROMS) coupled to a seven state variable (phytoplankton, zooplankton, nitrate, ammonium, small and large detritus, and chlorophyll) biological model, which has been used to study the nitrogen and carbon cycles of the US East Coast [*Fennel et al.*, 2006; *Hofmann et al.*, 2008].

The biological component of the model system is undergoing some upgrades, which include the inclusion of different sizes of phytoplankton and zooplankton, and dissolved organic matter (DOM). A 10-km resolution ROMS grid for the NorthEast North American (NENA) shelf was nested within the HYCOM North Atlantic (NA) basin grid. Nesting of the NENA domain within the NA model enables the capture of circulation features and variability in the regional domain that is forced in the NA basin. An analogous modeling approach could be used for the Patagonian shelf region.

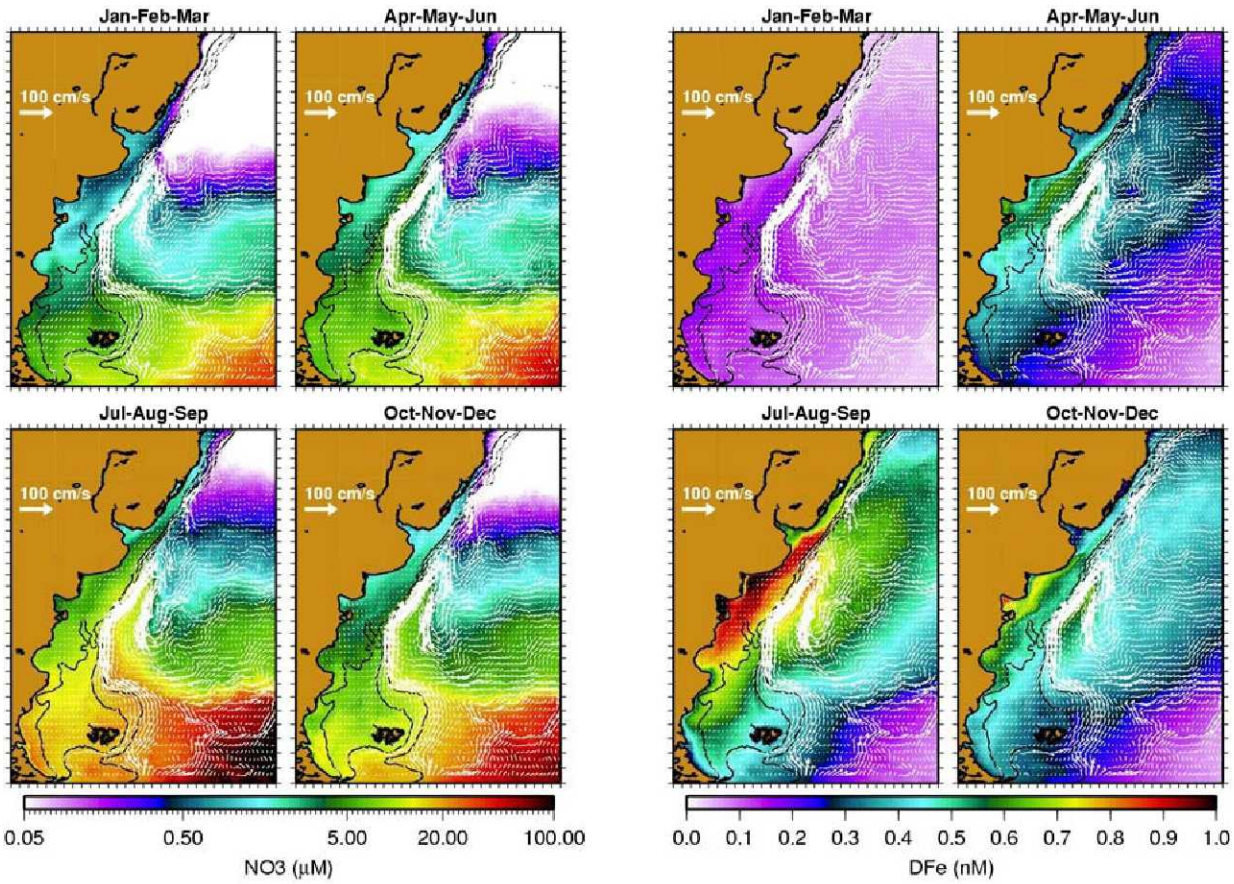

Figure 30. Empirically derived seasonal composites of surface nitrate (NO_3, left panel) and dissolved iron (DFe, right panel) using equations 13 and 14, and monthly MODIS Chl-a and SST.

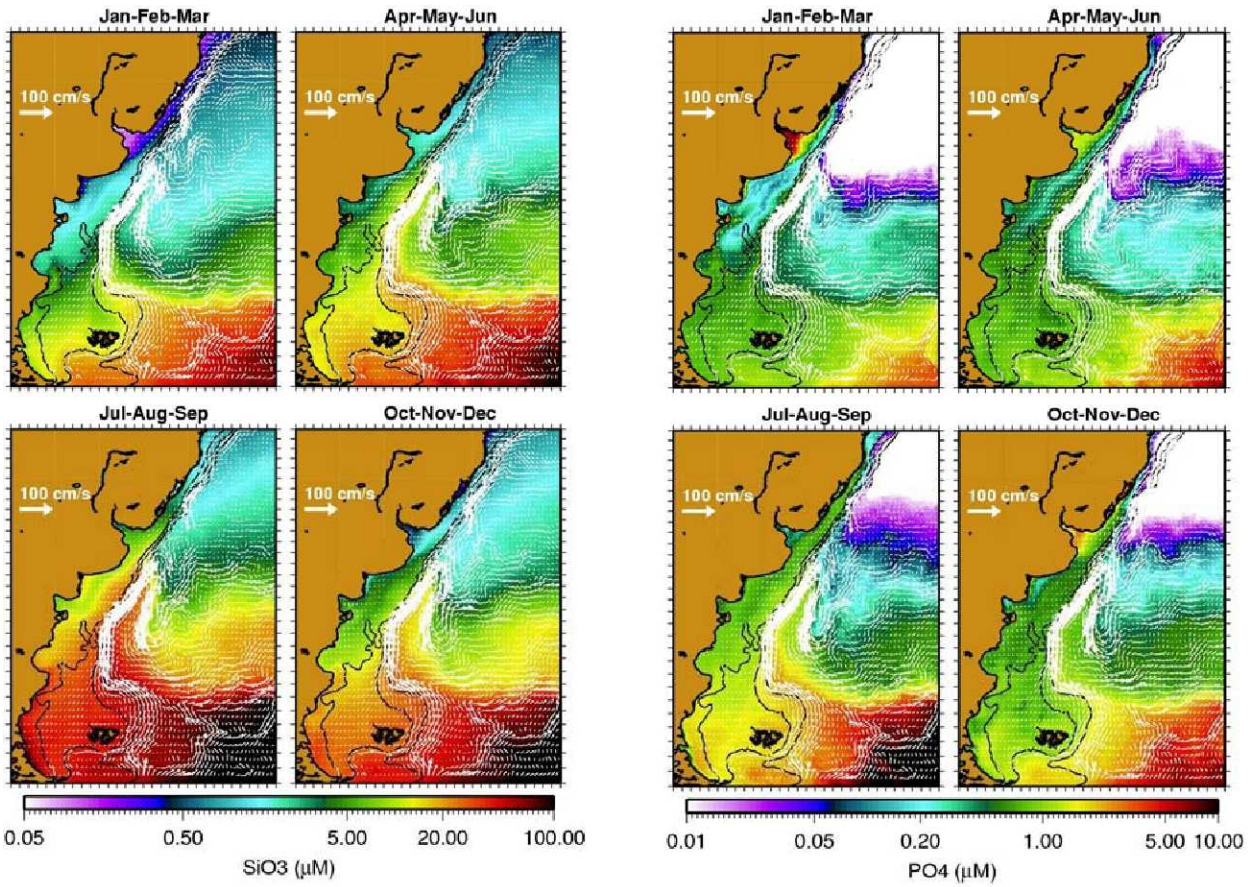

Figure 31. Empirically derived seasonal composites of surface silicate (SiO_3, left panel) and phosphate (PO_4, right panel) using equation 13, and monthly MODIS Chl-a and SST.

Acknowledgements. This work was funded by the NASA Ocean Biogeochemistry Program. This research was also partially funded by Grants 550370/02-1 (GOAL), 557305/05-5 (PATEX) and 520189/06-0 (SOS-CLIMATE) of the Brazilian Research Council (CNPq/MCT). We also thank the support given by the Brazilian Antarctic Program (PROANTAR) and the Brazilian Ministry of Environment (MMA). Partial support was also provided by grant CRN2076 from the Inter-American Institute for Global Change Research (IAI), which is supported by the US National Science Foundation (Grant GEO-0452325). We are thankful to Norman Kuring for helping in the identification of volcanic eruption data sources.

References

Acha, E.M., H.W. Mianzan, R.A. Guerrero, M. Favero, and J. Bava, Marine fronts at the continental shelves of austral South America Physical and ecological processes, *Journal of Marine Systems*, *44* (1-2), 83-105, 2004.

Austin, R.W., and T.J. Petzold, Spectral dependence of the diffuse attenuation coefficient of light in ocean waters, *Opt. Eng.*, *25*, 473-479, 1986.

Balch, W.M., H.R. Gordon, B.C. Bowler, D.T. Drapeau, and E.S. Booth, Calcium carbonate measurements in the surface global ocean based on Moderate-Resolution Imaging Spectroradiometer data, *Journal of Geophysical Research-Oceans*, *110* (C7), 2005.

Behrenfeld, M.J., E. Boss, D.A. Siegel, and D.M. Shea, Carbon-based ocean productivity and phytoplankton physiology from space, *Global Biogeochemical Cycles*, *19* (doi:10.1029/2004GB002299), 2005.

Bianchi, A.A., L. Bianucci, A.R. Piola, D.R. Pino, I. Schloss, A. Poisson, and C.F. Balestrini, Vertical stratification and air-sea CO_2 fluxes in the Patagonian shelf, *Journal of Geophysical Research-Oceans*, *110* (C7), 2005.

Bowie, A.R., D.J. Whitworth, E.P. Achterberg, R.F.C. Mantoura, and P.J. Worsfold, Biogeochemistry of Fe and other trace elements (Al, Co, Ni) in the upper Atlantic Ocean, *Deep-Sea Research Part I-Oceanographic Research Papers*, *49* (4), 605-636, 2002.

Brown, C.W., and G.P. Podesta, Remote sensing of coccolithophore blooms in the western South Atlantic Ocean, *Remote Sensing of Environment*, *60* (1), 83-91, 1997.

Brown, C.W., and J.A. Yoder, Coccolithophorid Blooms in the Global Ocean, *Journal of Geophysical Research-Oceans*, *99* (C4), 7467-7482, 1994.

Carreto, J.I., V.A. Lutz, M.O. Carignan, A.D.C. Colleoni, and S.G. Demarco, Hydrography and Chlorophyll-a in a Transect from the Coast to the Shelf-Break in the Argentinian Sea, *Continental Shelf Research*, *15* (2-3), 315-336, 1995.

Cassar, N., M.L. Bender, B.A. Barnett, S. Fan, W.J. Moxim, H. Levy, and B. Tilbrook, The Southern Ocean biological response to Aeolian iron deposition, *Science*, *317* (5841), 1067-1070, 2007.

Chassignet, E.P., H.E. Hulburt, O.M. Smedstad, G.R. Halliwell, P.J. Hogan, A.J. Wallcraft, and R. Bleck, Ocean prediction with the Hybrid Coordinate Ocean Model (HYCOM). in *Ocean Weather Forecasting: An Integrated View of Oceanography*, edited by E.P. Chassignet, and J. Verron, pp. 413-426, Springer, 2006.

Chassignet, E.P., H.E. Hurlburt, O.M. Smedstad, G.R. Halliwell, P.J. Hogan, A.J. Wallcraft, R. Baraille, and R. Bleck, The HYCOM (HYbrid Coordinate Ocean Model) data assimilative system, *Journal of Marine Systems*, *65* (1-4), 60-83, 2007.

Cheng, W., M.J. McPhaden, D.X. Zhang, and E.J. Metzger, Recent changes in the Pacific subtropical cells inferred from an eddy-resolving ocean circulation model, *Journal of Physical Oceanography*, *37* (5), 1340-1356, 2007.

Ciotti, A.M., C. Odebrecht, G. Fillmann, and O.O. Moller, Fresh-Water Outflow and Subtropical Convergence Influence on Phytoplankton Biomass on the Southern Brazilian Continental-Shelf, *Continental Shelf Research*, *15* (14), 1737-1756, 1995.

Duce, R.A., and N.W. Tindale, Atmospheric Transport of Iron and Its Deposition in the Ocean, *Limnology and Oceanography*, *36* (8), 1715-1726, 1991.

Erickson, D.J., J.L. Hernandez, P. Ginoux, W.W. Gregg, C. McClain, and J. Christian, Atmospheric iron delivery and surface ocean biological activity in the Southern Ocean and Patagonian region, *Geophysical Research Letters*, *30* (12), 2003.

Fennel, K., J. Wilkin, J. Levin, J. Moisan, J. O'Reilly, and D. Haidvogel, Nitrogen cycling in the Middle Atlantic Bight: Results from a three-dimensional model and implications for the North Atlantic nitrogen budget, *Global Biogeochemical Cycles*, *20* (3), 2006.

Franco, B.C., A.R. Piola, A.L. Rivas, A. Baldoni, and J.P. Pisoni, Multiple thermal fronts near the Patagonian shelf break, *Geophysical Research Letters* (doi:10.1029/2007GL032066), 2007, in press.

Gaiero, D.M., J.L. Probst, P.J. Depetris, S.M. Bidart, and L. Leleyter, Iron and other transition metals in Patagonian riverborne and windborne materials: Geochemical control and transport to the southern South Atlantic Ocean, *Geochimica Et Cosmochimica Acta*, *67* (19), 3603-3623, 2003.

Garcia, V.M.T., C.A.E. Garcia, M.M. Mata, R.C. Pollery, A.R. Piola, S.R. Signorini, C.R. McClain, and M.D. Iglesias-Rodriguez, High phytoplankton biomass and production along the Patagonian shelf-break (austral spring 2004), *Deep Sea Res. Part A*, *submitted*, 2007.

Gasso, S., and A.F. Stein, Does dust from Patagonia reach the sub-Antarctic Atlantic ocean?, *Geophysical Research Letters*, *34* (1), 2007.

Halliwell, G.R., Evaluation of vertical coordinate and vertical mixing algorithms in the HYbrid-Coordinate Ocean Model (HYCOM), *Ocean Modelling*, *7* (3-4), 285-322, 2004.

Hofmann, E., J.-N. Druon, K. Fennel, M.A.M. Friedrichs, D. Haidvogel, C. Lee, A. Mannino, C. McClain, R. Najjar, J.E. O'Reilly, D. Pollard, M. Previdi, S. Seitzinger, J. Siewert, S.R. Signorini, and J. Wilkin, Eastern US Continental Shelf Carbon Budget: Integrating Models, Data Assimilation, and Analysis, in *Oceanography*, pp. 86-104, 2008.

Kara, A.B., and H.E. Hurlburt, Daily inter-annual simulations of SST and MLD using atmospherically forced OGCMs: Model evaluation in comparison to buoy time series, *Journal of Marine Systems*, *62* (1-2), 95-119, 2006.

Kelly, K.A., L. Thompson, W. Cheng, and E.J. Metzger, Evaluation of HYCOM in the Kuroshio Extension region using new metrics, *Journal of Geophysical Research-Oceans*, *112* (C1), 2007.

Krishnamurthy, A., J.K. Moore, C.S. Zender, and C. Luo, Effects of atmospheric inorganic nitrogen deposition on ocean biogeochemistry, *Journal of Geophysical Research-Biogeosciences*, *112* (G2), 2007.

Lancelot, C., E. Hannon, S. Becquevort, C. Veth, and H.J.W. de Baar, Modeling phytoplankton blooms and carbon export production in the Southern Ocean: dominant controls by light and iron in the Atlantic sector in Austral spring 1992, *Deep Sea Res. I*, *47*, 1621-1662, 2000.

Luo, C., N.M. Mahowald, and J. del Corral, Sensitivity study of meteorological parameters on mineral aerosol mobilization, transport, and distribution, *Journal of Geophysical Research-Atmospheres*, *108* (D15), 2003.

Martin, G.H., S.E. Fitzwater, and R.M. Gordon, Iron deficiency limits phytoplankton growth in Antarctic waters, *Global Biogeochemical Cycles*, *4*, 4-12, 1990.

Matano, R.P., and E.D. Palma, The upwelling of downwelling currents, *Journal of Physical Oceanography*, submitted, 2008.

Meskhidze, N., A. Nenes, W.L. Chameides, C. Luo, and N. Mahowald, Atlantic Southern Ocean productivity: Fertilization from above or below?, *Global Biogeochemical Cycles*, *21* (2), 2007.

Moore, J.K., and O. Braucher, Sedimentary and mineral dust sources of dissolved iron to the world ocean, *Biogeosciences*, *5*, 631-656, 2008.

Moore, J.K., and S.C. Doney, Iron availability limits the ocean nitrogen inventory stabilizing feedbacks between marine denitrification and nitrogen fixation, *Global Biogeochemical Cycles*, *21* (2), 2007.

Moore, J.K., S.C. Doney, D.M. Glover, and I.Y. Fung, Iron cycling and nutrient-limitation patterns in surface waters of the World Ocean, *Deep-Sea Research Part Ii-Topical Studies in Oceanography*, *49* (1-3), 463-507, 2002a.

Moore, J.K., S.C. Doney, J.A. Kleypas, D.M. Glover, and I.Y. Fung, An intermidiate complexity marine ecosystem model for the global domain, *Deep Sea Res. II*, *49*, 403-462, 2002b.

Moore, J.K., S.C. Doney, and K. Lindsay, Upper ocean ecosystem dynamics and iron cycling in a global three-dimensional model, *Global Biogeochemical Cycles*, *18* (4), 2004.

Moore, J.K., S.C. Doney, K. Lindsay, N. Mahowald, and A.F. Michaels, Nitrogen fixation amplifies the ocean biogeochemical response to decadal timescale variations in mineral dust deposition, *Tellus Series B-Chemical and Physical Meteorology*, *58* (5), 560-572, 2006.

Morel, A., Optical modeling of the upper ocean in relation to its biogenous matter content (Case I Waters), *J. Geophys. Res.*, *93* (C9), 10,749-10,768, 1988.

Naranjo, J.A., and L.E. Lara, August-September 2003 small volcanian eruption at the Nevados de Chillán Volcanic Complex (36^{o} 50'S), Southern Andes (Chile), *Revista Geológica de Chile*, *31* (2), 359-366, 2004.

Nelson, D.M., and W.O. Smith, Sverdrup Revisited - Critical Depths, Maximum Chlorophyll Levels, and the Control of Southern-Ocean Productivity by the Irradiance-Mixing Regime, *Limnology and Oceanography*, *36* (8), 1650-1661, 1991.

Niencheski, L.F.H., H.L. Windom, W.S. Moore, and R.A. Jahnke, Submarine groundwater discharge of nutrients to the ocean along a coastal lagoon barrier, Southern Brazil, *Marine Chemistry*, *106* (3-4), 546-561, 2007.

Obata, A., J. Ishizaka, and M. Endoh, Global verification of critical depth theory for phytoplankton bloom with climatological in situ temperature and satellite ocean color data, *Journal of Geophysical Research-Oceans*, *101* (C9), 20657-20667, 1996.

Piola, A.R., E.J.D. Campos, O.O. Moller, M. Charo, and C. Martinez, Subtropical Shelf Front off eastern South America, *Journal of Geophysical Research-Oceans*, *105* (C3), 6565-6578, 2000.

Piola, A.R., and R.P. Matano, Brazil and Falklands (Malvinas) Currents, in *Encyclopedia of Ocean Sciences*, edited by J.H. Steele, K.K. Turekian, and S.A. Thorpe, pp. 340-349, Academic Press, New York, 2001.

Riley, G.A., Oceanography of Long Island Sound, 1952-54. 9. Production and utilization of organic matter, in *Bull. Bingham Oceanogr. Collect., 15*, pp. 324-343, 1956.

Rivas, A.L., Quantitative estimation of the influence of surface thermal fronts over chlorophyll concentration at the Patagonian shelf, *Journal of Marine Systems*, *63* (3-4), 183-190, 2006.

Rivas, A.L., A.I. Dogliotti, and D.A. Gagliardini, Seasonal variability in satellite-measured surface chlorophyll in the Patagonian Shelf, *Continental Shelf Research*, *26* (6), 703-720, 2006.

Saraceno, M., C. Provost, and A.R. Piola, On the relationship between satellite-retrieved surface temperature fronts and chlorophyll a in the western South Atlantic, *Journal of Geophysical Research-Oceans*, *110* (C11), 2005.

Siegel, D.A., S.C. Doney, and J.A. Yoder, The North Atlantic spring phytoplankton bloom and Sverdrup's critical depth hypothesis, *Science*, *296* (5568), 730-733, 2002.

Signorini, S.R., V.M.T. Garcia, A.R. Piola, C.A.E. Garcia, M.M. Mata, and C.R. McClain, Seasonal and interannual variability of calcite in the vicinity of the Patagonian shelf break (38 degrees S-52 degrees S), *Geophysical Research Letters*, *33* (16), 2006.

Signorini, S.R., and C. McClain, Further Studies on Oceanic Biogeochemistry and Carbon Cycling, pp. 51, NASA Goddard Space Flight Center, TM-2003-212245, Greenbelt, 2003.

Sverdrup, H.U., On conditions for the vernal blooming of phytoplankton, *J. Cons. Perm. Int. Explor. Mer*, *18*, 287-295, 1953.

Tegen, I., and I. Fung, Modeling of mineral dust in the atmosphere: Sources, transport, and optical thickness, *J. Geophys. Res.*, *99*, 22,897-22,914, 1994.

Timmermans, K.R., B. van der Wagt, and H.J.W. de Baar, Growth rates, half-saturation constants, and silicate, nitrate, and phosphate depletion in relation to iron availability of four large, open-ocean diatoms from the Southern Ocean, *Limnology and Oceanography*, *49* (6), 2141-2151, 2004.

Townsend, D.W., M.D. Keller, M.E. Sieracki, and S.G. Ackleson, Spring Phytoplankton Blooms in the Absence of Vertical Water Column Stratification, *Nature*, *360* (6399), 59-62, 1992.

Voss, K.J., A spectral model of the beam attenuation coefficient in the ocean and coastal areas, *Limnology and Oceanography*, *37* (3), 501-509, 1992.

Westberry, T., M.J. Behrenfeld, D.A. Siegel, and E. Boss, Carbon-based primary productivity modeling with vertically resolved photoacclimation, *Global Biogeochemical Cycles*, *22* (doi:10.1029/2007GB003078), 2008.

Windom, H.L., W.S. Moore, L.F.H. Niencheski, and R.A. Jahrike, Submarine groundwater discharge: A large, previously unrecognized source of dissolved iron to the South Atlantic Ocean, *Marine Chemistry*, *102* (3-4), 252-266, 2006.

Winther, N.G., and J.A. Johannessen, North Sea circulation: Atlantic inflow and its destination, *Journal of Geophysical Research-Oceans*, *111* (C12), 2006.

REPORT DOCUMENTATION PAGE

Form Approved
OMB No. 0704-0188

1. REPORT DATE *(DD-MM-YYYY)*	2. REPORT TYPE	3. DATES COVERED *(From - To)*
12-02-2009	Technical Memorandum	

4. TITLE AND SUBTITLE

Further Studies on the Physical and Biogeochemical Causes for Large Interannual Changes in the Patagonian Shelf Spring–Summer Phytoplankton Bloom Biomass

5a. CONTRACT NUMBER

5b. GRANT NUMBER

5c. PROGRAM ELEMENT NUMBER

6. AUTHOR(S)

Sergio R. Signorini, Virginia M.T. Garcia, Alberto R. Piola, Heitor Evangelista, Charles R. McClain, Carlos A.E. Garcia, and Mauricio M. Mata

5d. PROJECT NUMBER

5e. TASK NUMBER

5f. WORK UNIT NUMBER

7. PERFORMING ORGANIZATION NAME(S) AND ADDRESS(ES)

Goddard Space Flight Center
Greenbelt, MD 20771

8. PERFORMING ORGANIZATION REPORT NUMBER

200900836

9. SPONSORING/MONITORING AGENCY NAME(S) AND ADDRESS(ES)

National Aeronautics and Space Administration
Washington, DC 20546-0001

10. SPONSORING/MONITOR'S ACRONYM(S)

11. SPONSORING/MONITORING REPORT NUMBER

NASA TM–2009–214176

12. DISTRIBUTION/AVAILABILITY STATEMENT

Unclassified-Unlimited, Subject Catagory: 48
Report available from NASA Centerfor Aerospace Information, 7115 Standard Drive, Hanover, MD 21076. (301) 621-0390

13. SUPPLEMENTARY NOTES S.R. Signorini: SAIC, Beltsville, MD; V.M.T. Garcia: Federal University of Rio Grande, Rio Grande, Brazil; A.R. Piola: Universidad de Buenos Aires, Buenos Aires, Argentina; H. Evangelista: Universidade do Estado do Rio de Janeiro, Brazil; C.A.E. Garcia and M.M. Mata: Federal University of Rio Grande, Rio Grande, Brazil

14. ABSTRACT A very strong and persistent phytoplankton bloom was observed by ocean color satellites during September − December 2003 along the northern Patagonian shelf. The 2003 bloom had the highest extent and chlorophyll a (Chl-a) concentrations of the entire Sea-viewing Wide Field-of-view Sensor (SeaWiFS) period (1997 to present). SeaWiFS-derived Chl-a exceeded 20 mg m-3 in November at the bloom center. The bloom was most extensive in December when it spanned more than 300 km across the shelf and nearly 900 km north − south (35° S to 43° S). The northward reach and the deep penetration on the shelf of the 2003 bloom were quite anomalous when compared with other years, which showed the bloom more confined to the Patagonian shelf break (PSB). The PSB bloom is a conspicuous austral spring-summer feature detected by ocean color satellites and its timing can be explained using the Sverdrup critical depth theory. Based on high-resolution numerical simulations, in situ and remote sensing data, we provide some suggestions for the probable mechanisms responsible for that large interannual change of biomass as seen by ocean color satellites. Potential sources of macro and micro (e.g., Fe) nutrients that sustain the high phytoplankton productivity of the Patagonian shelf waters are identified, and the most likely physical processes that maintain the nutrient balance in the region are discussed.

15. SUBJECT TERMS

Ocean color, SeaWiFS, Modeling, Interannual Changes, Patagonian Shelf, Phytoplankton bloom biomass

16. SECURITY CLASSIFICATION OF:			17. LIMITATION OF ABSTRACT	18. NUMBER OF PAGES	19a. NAME OF RESPONSIBLE PERSON
a. REPORT	b. ABSTRACT	c. THIS PAGE			Charles R. McClain
Unclassified	Unclassified	Unclassified	Unclassified	43	19b. TELEPHONE NUMBER *(Include area code)* (301) 286-5377